NASA TN D-1743

NASA TN D-1743

TECHNICAL NOTE

D-1743

COMPARISON OF EXPERIMENTAL TO PREDICTED HEAT TRANSFER IN A BELL-SHAPED NOZZLE WITH UPSTREAM FLOW DISTURBANCES

By Anthony Fortini and Robert C. Ehlers

Lewis Research Center
Cleveland, Ohio

NATIONAL AERONAUTICS AND SPACE ADMINISTRATION
WASHINGTON August 1963

NATIONAL AERONAUTICS AND SPACE ADMINISTRATION

TECHNICAL NOTE D-1743

COMPARISON OF EXPERIMENTAL TO PREDICTED HEAT TRANSFER IN A BELL-SHAPED NOZZLE WITH UPSTREAM FLOW DISTURBANCES

By Anthony Fortini and Robert C. Ehlers

SUMMARY

An experimental investigation has been conducted to determine and compare the effects of upstream flow disturbances on the heat-transfer film coefficient in a Rao type nozzle with air at 300 pounds per square inch absolute and 1600° R. These disturbances caused a large change in the film coefficient and created difficulties for heat-transfer predictions. Two approaches are used for comparison, a boundary-layer model and a Nusselt number correlation method.

INTRODUCTION

Along with the advent of higher chamber pressure for the chemical rocket engine and the high heat fluxes encountered in the nuclear rocket engine, the marginality of cooling of these engines has become of great concern. In the past, gas-side heat-transfer film coefficients were obtained by assuming that one-dimensional heat-transfer correlations of the Nusselt number type were applicable. Physically, the application of one-dimensional correlations to the present-day bell-shaped rocket nozzles is not justified because the pressure, velocity, and temperature gradients are not one dimensional.

Bartz (ref. 1) developed an approximate boundary-layer solution for the heat-transfer problem by employing a one-dimensional flow field to a conical nozzle. As a means toward simplification, Bartz has also generated a Nusselt type correlation equation for a given conical nozzle contour (ref. 2). Since flow in a conical nozzle can be approximated by one-dimensionality, the question arises whether the simplified equation applies to a bell-shaped nozzle. Reference 3 has modified the boundary-layer solution of reference 1 by including an axisymmetric flow field (the flow pattern is the same in all meridian planes passing through the axis of symmetry, and the flow is two dimensional) and has compared the predictions (from ref. 3) with those from a Nusselt type correlation. The comparisons show large differences in heat flux.

In both references 1 and 3, it is assumed that the boundary layer was initially turbulent. There is a possibility that laminar flow may exist in the convergent and throat portions of the nozzle (e.g., ref. 4). References 1 and 3 have shown that their predictions of heat transfer in the convergent section are dependent on assumptions concerning the start of the turbulent boundary layer. However, they (refs. 1 and 3) show that these assumptions had little effect on the predictions of the divergent portion.

To establish a proper technique for calculating the local heat-transfer film coefficient, an experimental heat-transfer investigation was undertaken at the Lewis Research Center. This report presents (1) the test apparatus for heat-transfer measurements, (2) experimental measurements of the film coefficients and their comparison with the predictions of reference 3, and (3) some gross effects of upstream flow disturbances on the heat-flux distribution within the nozzle.

The experimental program utilized a truncated bell-shaped nozzle based on Rao's design (ref. 5). The design called for a nozzle area ratio of 27.28 but was truncated to an area ratio of 22.01. Heated, high-pressure air was the working fluid, and steady-state measurements of heat flux and wall temperatures were obtained by the use of plug-type heat-flux meters. Total pressure was held constant at 300 pounds per square inch absolute with a total temperature of 1600° R. Static wall pressure distributions were also obtained for each test condition.

SYMBOLS

C	constant of integration
$\bar{c}_p$	averaged specific heat at constant pressure
D	diameter
dt/dy	temperature gradient along shaft of heat-flux meter
h	heat-transfer film coefficient based on temperature
h_i	heat-transfer film coefficient based on enthalpy
i	enthalpy
k	thermal conductivity
k_0	intercept of conductivity data at 0° R
m	slope of conductivity data
P	static pressure
P_0	total pressure
q	heat flux
R	radius
T	static temperature

T_{ad}	adiabatic recovery temperature
T_w	nozzle wall temperature
T_O	total temperature
t	shaft temperature of heat-flux meter
V	velocity
x	longitudinal distance
y	distance along shaft of heat-flux meter
ϵ	area ratio
ρ	gas density
θ_c	angle of heat-flux meter location
θ_p	angle of pressure tap location

Subscripts:

ad	adiabatic recovery
t	throat
w	nozzle wall

APPARATUS

The equipment used for the test program consists of: (1) heat exchanger, (2) plenum chamber, (3) nozzle section, (4) nozzle cooling system, and (5) exhaust system. A schematic drawing of the apparatus is shown in figure 1.

Heat Exchanger

Dry, high-pressure air was heated while passing through a bank of parallel coils. These coils were heated by hot gases ejected from a jet-engine burner section. This scheme produced heated air at 300 pounds per square inch absolute and a temperature of 1600° R.

Plenum Chamber

The chamber (14-in. I.D. by 2 ft) was sized so that its cross-sectional area ratio relative to the nozzle throat was 74.2. With this area ratio and the use of one-dimensional flow equations, the plenum chamber was computed to have a gas velocity of 15.3 feet per second and static- to total-temperature and -pressure ratios of virtually 1.

Contained within the chamber is a flow-straightening structure made up of tubing 3/4 inch in outside diameter and 11 inches long. Ahead of the structure is a 15-inch-long diffuser section, which has an inlet inside diameter of 5 inches and an exit inside diameter of 14 inches. Although the chamber was not probed, the assumption was made that the combined grouping of diffuser and honeycomb produced a uniform flow field with stagnation conditions of 300 pounds per square inch absolute and 1600° R.

Nozzle Section

The operating conditions for the nozzle design were determined from the output of the heat exchanger. Total conditions were set at 300 pounds per square inch absolute and 1620° R, and the throat diameter was chosen to be 1.624 inches.

Geometrically, the nozzle consists of (1) a contraction portion with an inlet diameter of 7.63 inches and a contraction half-angle of 30°, (2) a convergent throat portion with a radius of curvature equal to the throat diameter, and (3) a divergent contoured portion starting at the throat. This divergent contour was determined by employing the method of reference 5 to which a boundary-layer displacement thickness was added. The nozzle was truncated from a diameter of 8.488 inches to a diameter of 7.624 inches, which resulted in an exit area ratio of 22.01. Table I shows a sketch of the nozzle and lists the nozzle coordinates.

Because of the high thermal stresses imposed on the nozzle and the requirement of a high temperature gradient through the wall, stainless-steel 304 was selected as the nozzle material. The nozzle was then machined from a forged billet so that the wall thickness was 0.5 inch, which was set by the size of the heat-flux meters.

Two devices were inserted in the nozzle section for an overall study of flow disturbances on the heat-transfer film coefficient. The first device was a V-gutter turbulence generator, as shown in figure 2, located in the convergent section 3.38 inches upstream of the throat. The second device simulated a nuclear-core reactor whose geometry is depicted in figure 3. The exit face of the reactor was located at 0.85 inch ahead of the contraction section of the nozzle. Both of these devices not only generated a turbulence level but also altered the boundary-layer characteristics.

Nozzle Cooling

Cooling of the nozzle was achieved by a water bath that acted as a heat sink. Sufficient water was added continuously to the bath in order to maintain a constant outlet water temperature that was essentially equal to the inlet temperature.

Exhaust System

The nozzle was attached to an exhaust tube 24 inches in diameter, which, in turn, was connected to an exhauster system. Under flow conditions, the exhausters were capable of maintaining a nozzle back pressure of 2 pounds per square inch absolute.

INSTRUMENTATION

Direct basic measurements made were pressure and temperature. Indirect measurements were heat flux and inside nozzle-wall temperatures. Coordinates of the instrumentation location are given in table I.

Pressure

The plenum-chamber total pressure and the first seven nozzle-wall pressures were measured with Bourdon tube pressure gages. The range of these gages was selected such that the error in measurement was less than 1/2 of 1 percent of full scale. Manometers were used for the remaining wall pressures and connected in a differential fashion. Manometer fluids used were mercury, acetylene tetrabromide, and dibutyl phthalate. These fluids were calibrated for density against temperature to reduce manometer errors. An average manometer board temperature was measured, and this value was used to determine the manometer fluid density. All other manometer errors were considered negligible. Reading error of the meniscus was determined to be 0.05 inch.

Temperature

Steady-state measurements of inside wall temperature and local heat flux were obtained by an Inconel plug-type heat-flux meter (fig. 4(a)). The diameter of the meter shaft was 0.125 inch, and three Chromel-Alumel thermocouples were accurately located and peened into the shaft. After attachment, the thermocouples were wrapped around the shaft to reduce the error in temperature measurement because of heat conduction along the 0.008-inch-diameter thermocouple wire.

A typical plot of temperature against thermocouple location is also shown in figure 4(b). By extrapolation of the three thermocouple readings, an inside nozzle-wall temperature could be obtained. The heat flux through the plug was calculated by the use of the temperature distribution of the plug and the known thermal conductivity of the Inconel. Three samples of Inconel from which the plugs were made were calibrated for thermal conductivity by Battelle Memorial Institute, and the data are presented in figure 5.

PROCEDURE

For each test condition, total pressure and temperature were held constant at a nominal condition of 300 pounds per square inch absolute and 1600° R, respectively. These conditions were obtained after the heat exchanger had reached a stable state. Cooling water to the nozzle bath was also maintained at a steady state such that the temperature rise across the bath was less than 5° F. The meters were then monitored until steady-state conditions were established.

All data were recorded during a steady-state time interval of 15 minutes. Each temperature was recorded 10 times by an automatic voltage digitizer. The manometer board was photographed 10 times during the same time period, but Bourdon gages were read only once. The purpose of recording the same data 10 times was to ensure that steady-state conditions existed and to average out any of the small recording and reading errors.

ANALYSIS OF EXPERIMENTAL DATA

This section of the report discusses the experimental data along with its reduction and gives a comparison of the nozzle pressure and mass flux distribution with that predicted by theory.

Nozzle Pressure Distribution

In the design of the nozzle, the flow field was assumed to be symmetrical about the longitudinal axis and to consist of two regions. For the subsonic region (convergent portion), the assumed flow was one dimensional; whereas, for the supersonic region (divergent portion), the assumed flow was axisymmetric. The axisymmetric field was computed by applying the method of characteristics and the optimization technique of reference 5. The characteristic net calculations were initiated by determining a constant Mach line in the vicinity of the throat. The transonic analysis of reference 6 was used to obtain the Mach line.

Nozzle coordinates were computed by adding a boundary-layer displacement thickness to the nonviscous flow field. A detailed explanation for the viscous part of this nozzle design is given in reference 3. Some of these nozzle coordinates are presented in table I with their associated instrumentation location.

The theoretical pressure distribution associated with the edge of the nonviscous flow field is shown in figure 6 as a solid line. As would be expected, a discontinuity exists at the throat region because of the two different theoretical flow fields.

Also presented in figure 6 is the measured pressure distribution for the condition of no upstream flow disturbance. Pressure distributions for the turbulence generator and nuclear-core simulator were the same (within measurement accuracy) as with no flow disturbance, because the upstream disturbances did not materially alter the boundary-layer development insofar as pressure distribution is concerned. Hence, the experimental data of figure 6 would be representative of the aforementioned upstream flow disturbances. Static-pressure drop across the turbulence generator and the reactor core amounted to less than 2 percent of the total pressure.

The experimental data shown in figure 6 are in good agreement with theory except for the throat and exit sections of the nozzle. For the convergent section near the throat region, the experimental data should depart from theory because of the transition from one-dimensional to axisymmetric flow. At the throat, the experimental data seem to indicate that the method of reference 6 is not adequate for a nozzle that has a small radius of curvature. The deviation from theory for the data just after the throat should be expected, since this method was employed as the initial condition. For the exit region of the nozzle, the experimental data fall below the theoretical line indicating a thinner boundary layer than that predicted by theory. Again, for this portion of the nozzle, the theory could be in error because of some of the assumptions used in predicting the boundary-layer growth rate.

Although the back pressure was greater than the nozzle-exit pressure, figure 6 shows that neither strong shocks nor flow separation were encountered within the nozzle. From the smoothness of the experimental data, indications are that the flow field was adequate to perform the desired heat-transfer measurements and to determine the boundary-layer film coefficient.

Mass Flux Distribution

It is suggested in reference 2 that the film coefficient is proportional to the mass flux ρV raised to some power. To compare the experimental calculated values of mass flux distribution with theory, figure 7 is presented. The experimental values were determined by using the experimental pressure ratio and the tables of reference 7. Here again, the experimental data agree well with theory except for the throat region. The percent error from theory for the mass flux and the pressure ratio distributions are presented in table II.

Wall Temperature Distribution

The heat-flux meter shown in figure 4(a) provided a means of determining the inside nozzle-wall temperature and the heat flux at a local point. This technique was dependent on a theoretical temperature distribution derived from Fourier's heat-conduction equation. The assumptions used were one-dimensional heat flux, steady-state conditions, and a linear variation of thermal conductivity with temperature. For these assumptions, a simple integration of $q = -(mt + k_0)dt/dy$ yields a temperature distribution along the shaft of the meter. The distribution is $-qy = (mt^2/2) + k_0 t + C$. Since location and temperature at a point along the shaft are measured, the remaining unknowns are q and C, because m and k_0 can be determined from the thermal conductivity data of figure 5. Substitution of y and t for two of the three locations results in determining q and C over that interval. If the three points did not fit the distribution function exactly, three values of q and C were computed. The values of q were arithmetically averaged, and the values of C were used in computing three inside nozzle-wall temperatures by letting $y = 0$. These temperatures were also averaged.

Three runs (1 to 3) were made to investigate reproducibility of the meters. These runs had no upstream flow disturbance, and the total pressure was held constant at 300 pounds per square inch absolute. The total temperatures for runs 1, 2, and 3 were 1593°, 1607°, and 1622° R, respectively.

Table III is presented to show the reproducibility of the temperatures along the meter shaft for runs 1 to 3. Station 8 shows a large deviation from the average, which is due to an intermittent short in thermocouple C of the third run. If station 8 is neglected, the reproducibility in temperature measurement is within ±4.5 percent. The dashes in the table represent thermocouples that were broken during installation of the meter.

Wall temperature distributions of the nozzle for the three conditions of flow disturbance are plotted in figures 8(a) to (d). These figures show the data points to consist of a bar and a triangle. The bar symbolizes the span obtained by applying combinations of two out of the three thermocouples in the temperature-distribution equation. The triangle symbolizes the average of the three extrapolated wall temperatures resulting from the combination technique. Whenever the span was small, the average of three values is plotted. For the meters that had a broken thermocouple, only one wall temperature could be extrapolated and is depicted by a square symbol.

Figure 8(a) shows a typical wall temperature distribution for one of the three runs having no flow disturbance. A curve was drawn through the average values except when judicially selected values of the span were used because of large deviations about the average. If the thermocouple were attached properly, the span should remain constant from run to run provided that the total conditions were held fixed. Variation in span at a station is assumed to be caused by the oxidation film of the thermocouple ball and the contact resistance of the ball as a result of peening. Large deviation of the data from the faired curve is believed to be due to shorted thermocouples or electrical errors in the recording equipment.

For runs 1 to 3, the average wall temperatures at a station are plotted in figure 8(b). This figure shows that reproducibility is poor for stations 4, 8, 11, 12, 17, 18, and 19. No attempt was made to improve their reproducibility for fear of damaging other meters in the process of removal. Also, it was felt that the malfunction of these meters was not detrimental in determining a curve through the data except for station 4. All other stations indicated good reproducibility.

It should also be pointed out that the mathematically extrapolated wall temperature obtained from the temperature-distribution equation depends on the value of C, the integration constant. The magnitude of C is related to q, and q is proportional to the slope at a point on the temperature-distribution curve of the meter. Therefore, if the slope is in error because of a faulty temperature reading, C is in error accordingly. It was shown in table III that the reproducibility of the meter temperatures was within ±4.5 percent except for station 8. Figure 8(b) shows that the spread of the averaged wall temperatures at a station falls within the same band of reproducibility.

The wall temperature distributions of the nozzle having upstream flow disturbances are shown for the nuclear-core simulator (fig. 8(c)) and for the turbulence generator (fig. 8(d)). In figure 8(d), the curve was not drawn through the data of station 1 because of its nearness in location to the turbulence generator.

Heat-Transfer Film Coefficient

Experimental values of film coefficient based on enthalpy were determined by use of the following equation:

$$h_i = \frac{h}{c_p} = \frac{q}{i_{ad} - i_w}$$

The enthalpy difference can be expressed as $i_{ad} - i_w = \int_w^{ad} c_p \, dT$. Since c_p is approximately constant over the range of temperatures, then $i_{ad} - i_w \approx \bar{c}_p(T_{ad} - T_w)$ where $\bar{c}_p$ was computed by arithmetically averaging the specific heats determined at adiabatic and wall temperatures. The adiabatic wall temperature t_{ad} was computed by using a 0.9 recovery factor for the gas at the edge of the nonviscous flow field. Thermal properties of the gas were obtained from reference 8. A listing of the ratios of theoretical static to total temperature and adiabatic recovery temperature to total temperature is given in table IV. Also presented is the equation used in computing the ratio of adiabatic recovery temperature to total temperature.

As discussed previously, the meter produced three values of wall temperature and heat flux depending on which combination of two out of three thermocouples was used. Substitution of these combinations into the preceding equation results in three values for the film coefficient at one station. From the three values, an average film coefficient was computed.

Heat-transfer film coefficients for the nozzle with and without upstream flow disturbances are presented in figures 9(a) to (d). The bar shown in these figures represents the span of the three values of film coefficient, and the triangular symbol denotes the average. The square symbol is used when only one value of the film coefficient could be computed because of an open thermocouple. Again, each curve is faired through the average whenever possible.

The data of figure 9(a) are for the same total and flow conditions as in figure 8(a). Figure 9(a) shows that, if those stations that have poor wall temperature reproducibility are deleted, the maximum span of the film coefficient at a station is 40 percent. This large span was traced to the sensitivity of q in the extrapolation technique of the temperature distribution along the shaft of the heat-flux meter.

Reproducibility of the data for runs 1 to 3 is shown in figure 9(b), where the average values of film coefficient for each of the three runs are plotted. If all station points that were not reproducible as previously discussed are excluded, the band of reproducibility of the average is ±15 percent for station 3 and less than ±10 percent for all others.

Data for the core simulator and turbulence generator are shown in figures 9(c) and (d), respectively.

COMPARISON OF EXPERIMENTAL RESULTS

As a means of comparison, a composite plot of the film coefficient for the three upstream flow disturbances is given in figure 9(e). The curves of figure 9(e) are those of figures 8(b) to (d). For each curve, the maximum value of the film coefficient occurs ahead of the throat. This throat distribution is quite similar to that presented in reference 9 for a hydrazine - nitrogen tetroxide rocket thrustor. If the experimental pressure distribution (fig. 6) and mass flux distribution (fig. 7) are considered along with the suggestion of reference 2 that the film coefficient is proportional to the mass flux raised to a power, the maximum should occur ahead of the throat.

From a comparison of the curves, it is apparent that the level of the maximum varies. Reference 10 shows that increasing the free-stream turbulence affects local rates of heat transfer. Since the turbulence generator gives the highest turbulence level with a corresponding greatest maximum wall temperature level for the three flow conditions, the trend is in the right direction. However, a word of caution must be used in deriving a conclusion about turbulence level. Not only did the devices inserted into the nozzle increase the turbulence level, but they also simultaneously altered the boundary-layer characteristics from those of the test with no upstream disturbance.

If the reader is cognizant of the gross effects of the devices, a comparison of the curves shows that the largest differences in film coefficient occur in the convergent portion of the nozzle. As the flow approaches the throat region, this difference decreases. When the exit is reached, the three curves, in essence, are equal. Hence, the observation made is that the throat has a tendency to attenuate the effects of turbulence level.

For the turbulence generator, the value of the film coefficient just upstream of the throat is 55 percent greater than that for no flow disturbance. In comparison with the nuclear-core simulator, this difference amounts to 25 percent.

COMPARISON WITH PREDICTION TECHNIQUES

Two prediction methods are used for comparison with the experimental data. The first is a boundary-layer approach, as presented in reference 3; the second is a turbulent Nusselt type correlation, as used in reference 3.

In figure 9(f), the results of the two prediction methods are presented along with the experimental averaged curve of film coefficient for the condition of no upstream flow disturbance. In the boundary-layer curve for the plain nozzle, as presented in this figure, it is assumed that the boundary layer starts in the plenum chamber at the exit of the straightening tubes, which is 42.61 inches upstream of the nozzle throat.

In the convergent section, the experimental data fall above both prediction curves but follow the boundary-layer curve near and at the throat section. After the throat, the data agree with the Nusselt type correlation but cross over to the boundary-layer curve in the divergent portion of the nozzle.

Since the two prediction curves have at most a difference of 20 percent, the correlation method seems adequate as a first approximation for nozzle heat-transfer design except for the far upstream convergent section.

The curve for the experimental data of the nuclear-core simulator, as shown in figure 9(c), is again presented in figure 9(g) for the purpose of comparison with predictions. In the boundary-layer method, three boundary-layer starting points were computed to determine which starting point resulted in the best agreement with the experimental data. These starting points were 0, 5, and 10 inches upstream of the reactor exit face. It was convenient to assume that the boundary layer started ahead of the reactor exit, so that an effective boundary-layer height existed after the reactor exit. Best agreement with the experimental data was for the 10-inch starting point, and this boundary-layer curve is shown in figure 9(g). Also presented in the figure is the Nusselt type correlation.

Figure 9(g) shows that the two prediction methods underestimate the experimental data for the convergent section of the nozzle; but, at the throat and slightly downstream, the Nusselt type correlation seems to be adequate. In the divergent section, the data depart from the correlation method toward the boundary-layer method.

Because the experimental data just after the throat fall between the two methods and their differences are not large, the designer may again select the Nusselt type correlation for a first estimate over this region of the nozzle.

Curves for the turbulence generator test are presented in figure 9(h). Shown in the figure is the experimental curve of figure 9(d). The prediction curves, Nusselt type correlation and boundary-layer approach, employed the same models as discussed in figure 9(g). Again, three boundary-layer starting points were assumed, and the best agreement with experimental data occurs when the 10-inch upstream starting point is used.

Both prediction methods underestimate the experimental film coefficient for the convergent and throat portions of the nozzle by about 40 percent. Just beyond the throat, the experimental curve agrees well with the boundary-layer approach; however, here again the designer can use the Nusselt type correlation for first estimates.

By observing the peaks of the three experimental curves relative to their respective prediction curves, it is noted that the peak differences increase in magnitude as the turbulence level increases.

SUMMARY OF RESULTS

An experimental investigation has been conducted for the determination and comparison of the heat-transfer film coefficient in a truncated Rao type nozzle. This nozzle was operated with dry air heated to 1600° R and at a pressure of 300 pounds per square inch absolute. Two devices, a nuclear-core simulator and a turbulence generator, were inserted upstream of the nozzle throat to produce flow disturbances. Under these disturbances, measurements of film coefficient were obtained and compared with each other as well as with two prediction methods, namely, a boundary-layer approach and a Nusselt type correlation.

An analysis of the results generates the following statements:

1. Experimental measurements of the nozzle-wall pressure distributions agreed well with theory except for the throat region. The flow field follows a one-dimensional model for the convergent region and an axisymmetric model for the divergent region. Disagreement at the throat region is attributed to the method used in predicting the sonic region of the throat.

2. Upstream flow disturbances strongly affect the film coefficient in the convergent and throat regions of the nozzle. Acting as a choke, the throat dampened the disturbance essentially to zero for a large portion of the divergent section. The turbulence generator increased the film coefficient near the throat by 55 percent of the value with no disturbance; the reactor-core simulator gave 25 percent increase.

3. For the three tests with no upstream disturbance, core simulator, and turbulence generator, either prediction method may be used for design purposes. The best agreement is with the boundary-layer method. However, the far upstream convergent section is not in agreement with either prediction method.

4. The outstanding difficulties with the prediction methods are (1) assumptions have to be made regarding the start of the turbulent boundary layer in order that the experimental data fit the predictions made by the boundary-layer method, and (2) turbulence intensity and scale are not accounted for in either method.

Lewis Research Center
National Aeronautics and Space Administration
Cleveland, Ohio, May 7, 1963

REFERENCES

1. Bartz, Donald R.: An Approximate Solution of Compressible Turbulent Boundary-Layer Development and Convective Heat Transfer in Convergent-Divergent Nozzles. Trans. ASME, vol. 77, no. 8, Nov. 1955, pp. 1235-1245.

2. Bartz, Donald R.: A Simple Equation for Rapid Estimation of Rocket Nozzle Convective Heat Transfer Coefficients. Jet Prop., vol. 21, no. 1, Jan. 1957, pp. 49-51.

3. Neumann, H. E., and Bettinger, P. J.: A Comparative Analysis of Convective Heat Transfer in a Nuclear Rocket Nozzle. NASA TN D-1742, 1963.

4. Wegener, P., et al.: NOL Hypersonic Tunnel No. 4 Results V: Experimental and Theoretical Investigation of a Cooled Hypersonic Wedge Nozzle. NAVORD Rep. 2701, Naval Ordnance Lab., Apr. 13, 1953.

5. Rao, G. V. R.: Exhaust Nozzle Contour for Optimum Thrust. Jet Prop., vol. 28, no. 6, June 1958, pp. 377-382.

6. Sauer, R.: General Characteristics of the Flow Through Nozzles at Near Critical Speeds. NACA TM 1147, 1947.

7. Ames Research Staff: Equations, Tables, and Charts for Compressible Flow. NACA Rep. 1135, 1947. (Supersedes NACA TN 1428.)

8. Hilsenrath, Joseph, et al.: Tables of Thermal Properties of Gases. Cir. 564, NBS, Nov. 1, 1955.

9. Welsh, William E., Jr., and Witte, Arvel B.: A Comparison of Analytical and Experimental Local Heat Fluxes in Liquid-Propellant Rocket Thrust Chambers. TR 32-43, Jet Prop. Lab., C.I.T., Feb. 1, 1961.

10. Kestin, J., and Maeder, P. F.: Influence of Turbulence on Transfer of Heat from Cylinders. NACA TN 4018, 1957.

TABLE I. - NOZZLE CONTOUR AND COORDINATES

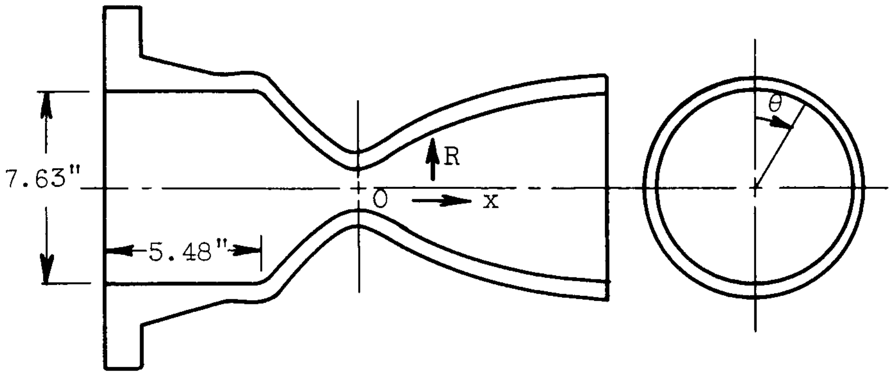

Pressure tap	Heat-flux meter	Angle of pressure tap, θ_p, deg	Angle of heat-flux meter, θ_c, deg	Longitudinal distance, x, in.	Radius, R, in.
1	1	180	0	-3.078	2.336
2	2	282.86	102.86	-.808	1.025
3	3	231.43	51.43	-.549	.898
4	4	180	0	-.273	.831
5	5	128.58	308.58	.081	.816
6	6	77.15	257.15	.150	.823
7	7	25.72	205.72	.300	.866
8	8	334.29	154.29	.536	.971
9	9	282.86	102.86	1.532	1.420
10	10	231.43	51.43	2.540	1.823
11	11	180	0	3.534	2.166
12	12	128.58	308.58	4.568	2.470
13	13	231.43	51.43	5.542	2.724
14	14	180	0	6.541	2.951
15	15	128.58	308.58	7.544	3.153
16	16	231.43	51.43	8.543	3.333
17	17	180	0	9.553	3.395
18	18	128.58	308.58	10.548	3.637
19	19	180	0	11.347	3.746
Exit	--	------	------	11.890	3.813

TABLE II. - COMPARISON OF EXPERIMENTAL AND THEORETICAL PERFORMANCE OF A RAO NOZZLE WITH DRY AIR

[Total pressure, 300 lb/sq in. abs; total temperature, 1600° R.]

Station	Ratio of longitudinal distance to throat diameter, x/D_t	Area ratio, ϵ	Pressure ratio, P/P_0			Mass flux, ρV, $lb_{mass}/(ft^2)(sec)$		
			Theoretical	Experimental	Error, percent	Theoretical	Experimental	Error, percent
Convergent section, one-dimensional flow								
1	-1.894	8.2762	0.9966	0.9956	-0.10	68.67	80.31	16.95
2	-.497	1.5919	.8959	.8997	.42	358.8	353.0	-1.62
3	-.338	1.2217	.8002	.7805	-2.46	467.6	483.5	3.40
4	-.168	1.0461	.6677	.6145	-7.97	555.2	561.8	1.19
Divergent section, axisymmetric flow								
5	0.050	1.0099	0.2772	0.3798	37.01	489.0	543.4	11.12
6	.092	1.0260	.2267	.2831	24.88	449.5	493.0	9.68
7	.185	1.1374	.1284	.1517	18.15	393.3	370.4	9.17
8	.330	1.4300	.1036	.1048	1.16	301.8	303.7	.63
9	.943	3.0582	.04955	.05074	2.40	195.9	198.7	1.43
10	1.563	5.0404	.02854	.02911	2.00	139.0	140.7	1.22
11	2.175	7.1155	.01896	.01925	1.53	107.0	108.0	.93
12	2.811	9.2530	.01358	.01353	-.37	86.09	85.89	-.23
13	3.410	11.2497	.01048	.01055	.67	72.60	72.92	.44
14	4.025	13.2032	.008379	.008424	.54	62.58	62.81	.37
15	4.642	15.0729	.006910	.006807	-1.49	55.03	54.48	-1.00
16	5.257	16.8484	.005846	.005678	-2.87	49.20	48.24	-1.95
17	5.879	18.5260	.005035	.004898	-2.72	44.50	43.68	-1.84
18	6.491	20.0620	.004419	.004216	-4.59	40.74	39.47	-3.12
19	6.983	21.2825	.004021	.003829	-4.77	38.23	36.98	-3.27

TABLE III. - SHAFT TEMPERATURES OF HEAT-FLUX METER

[Total pressure, 300 lb/sq in. abs.]

Station	Shaft temperature, °R, for run -									Average shaft temperature, °R			Deviation from average, percent, for run -								
	1 (Total temperature, 1593° R)			2 (Total temperature, 1607° R)			3 (Total temperature, 1622° R)						1			2			3		
	Thermocouple																				
	A	B	C	A	B	C	A	B	C	A	B	C	A	B	C	A	B	C	A	B	C
1	957.65	867.22	783.24	941.30	851.56	768.74	956.57	866.86	783.24	951.84	861.88	776.41	0.610	0.619	0.620	-1.11	-1.20	-1.24	0.496	0.578	0.620
2	1166.2	1064.9	924.13	1153.4	1044.7	890.87	1174.5	1070.2	926.02	1164.7	1059.9	913.67	.129	.472	1.14	-.968	-1.43	-2.50	.841	.971	1.35
3	1193.3	1056.8	895.00	1191.5	1050.4	857.68	1202.4	1067.2	919.91	1195.7	1058.1	890.86	-.201	-.122	.465	-.351	-.728	-3.72	.560	.860	3.26
4	1167.8	1054.4	925.54	1201.0	1076.4	935.90	1197.0	1079.6	945.43	1188.6	1070.1	935.62	-1.75	-1.47	-1.08	1.04	.589	.030	.707	.888	1.05
5	1188.6	1077.1	935.28	1175.8	1060.3	918.83	1194.4	1081.4	937.83	1186.3	1072.9	930.65	.194	.391	.498	-.885	-1.17	-1.27	.683	.792	.772
6	1178.8	1069.6	940.04	1156.9	1050.8	926.02	1184.9	1073.9	942.45	1173.5	1064.8	936.17	.452	.451	.413	-1.41	-1.31	-1.08	.971	.855	.671
7	1121.2	1016.6	886.46	1093.6	981.84	841.48	------	1017.4	884.12	1107.4	1005.3	870.69	1.25	1.12	1.81	-1.25	-2.33	-3.35	----	1.20	1.54
8	1107.6	------	899.50	1084.4	-------	855.43	1111.5	-------	515.00	1101.2	-------	756.66	.581	------	18.9	-1.53	------	13.05	.935	-----	-31.9
9	1001.8	922.27	836.62	995.83	913.51	830.23	1006.5	924.40	837.79	1001.4	920.06	834.88	.0399	.240	.208	-.556	-.712	-.557	.509	.472	.349
10	929.79	862.09	783.33	926.92	861.01	785.04	933.84	866.60	787.92	930.18	863.23	785.43	-.0419	-1.32	-.267	-.350	-.257	-.050	.393	.390	.317
11	873.33	808.09	735.40	865.58	797.11	719.65	873.15	857.08	732.34	870.69	820.76	729.13	.303	-1.54	.860	-.587	-2.88	-1.30	.283	4.425	.440
12	863.53	771.26	710.18	882.92	761.44	702.10	846.70	769.82	707.48	864.38	767.51	706.59	-.098	.489	.508	2.14	-.791	-.635	-2.05	.301	.126
13	-------	743.29	692.45	-------	736.84	685.67	-------	747.39	695.86	-------	742.51	691.33	------	.105	.162	------	-.764	-.819	------	.657	.655
14	752.16	-------	663.97	743.85	-------	655.56	751.80	-------	663.29	749.27	-------	661.94	.386	------	.307	-.723	------	-.511	.338	-----	.204
15	740.36	701.28	659.64	731.53	694.87	655.98	747.39	707.57	666.35	739.76	701.24	660.66	.081	.006	-.154	-1.11	-.908	-.708	1.03	.903	.861
16	708.26	677.26	637.58	700.83	669.22	629.20	710.61	679.55	639.62	706.57	675.34	635.47	.239	.284	.332	-.812	-.906	-.987	.572	.623	.653
17	-------	651.64	619.20	-------	650.04	595.37	-------	657.08	591.83	-------	652.92	602.13	------	-.196	2.83	------	-.441	-1.12	------	.637	-1.71
18	654.78	621.63	594.41	672.58	645.58	594.66	676.90	649.00	616.69	668.09	638.74	601.92	-1.99	-2.68	-1.25	.672	1.07	-1.21	1.32	1.61	2.45
19	646.44	619.99	590.45	666.36	637.24	605.92	670.27	640.73	607.63	661.02	632.65	601.33	-2.21	-2.00	-1.81	.808	.726	.763	1.40	1.28	1.05

TABLE IV. - THEORETICAL PERFORMANCE OF A RAO NOZZLE

Station	Ratio of longitudinal distance to throat diameter, x/D_t	Theoretical temperature ratio, T/T_0	Theoretical recovery temperature ratio, T_{ad}/T_0 (a)
Convergent section, one-dimensional flow			
1	-1.894	0.9990	0.9999
2	-.497	.9691	.9969
3	-.338	.9383	.9938
4	-.168	.8910	.9891
Divergent section, axisymmetric flow			
5	0.050	0.7128	0.9713
6	.092	.6748	.9675
7	.185	.5772	.9577
8	.330	.5438	.9544
9	.943	.4421	.9442
10	1.563	.3780	.9378
11	2.175	.3364	.9336
12	2.811	.3078	.9308
13	3.410	.2838	.9284
14	4.025	.2662	.9266
15	4.642	.2518	.9252
16	5.257	.2400	.9240
17	5.879	.2300	.9230
18	6.491	.2215	.9222
19	6.983	.2156	.9216

[a] $T_{ad}/T_0 = 0.9 + 0.1\ T/T_0$ where 0.9 = recovery factor.

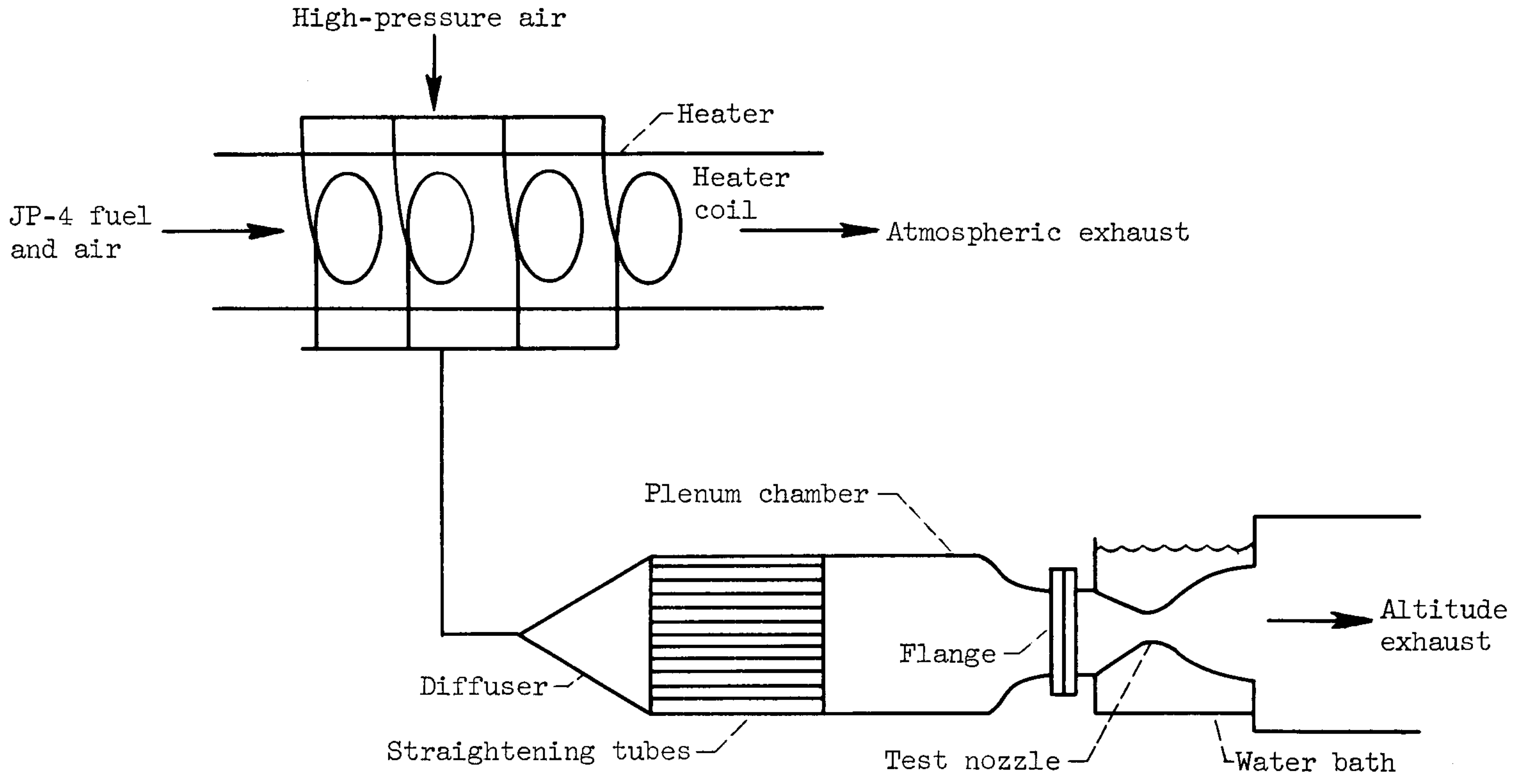
High-pressure air
Heater
Heater coil
JP-4 fuel and air
Atmospheric exhaust
Plenum chamber
Altitude exhaust
Flange
Diffuser
Straightening tubes
Test nozzle
Water bath

Figure 1. - Schematic drawing of heat-transfer facility.

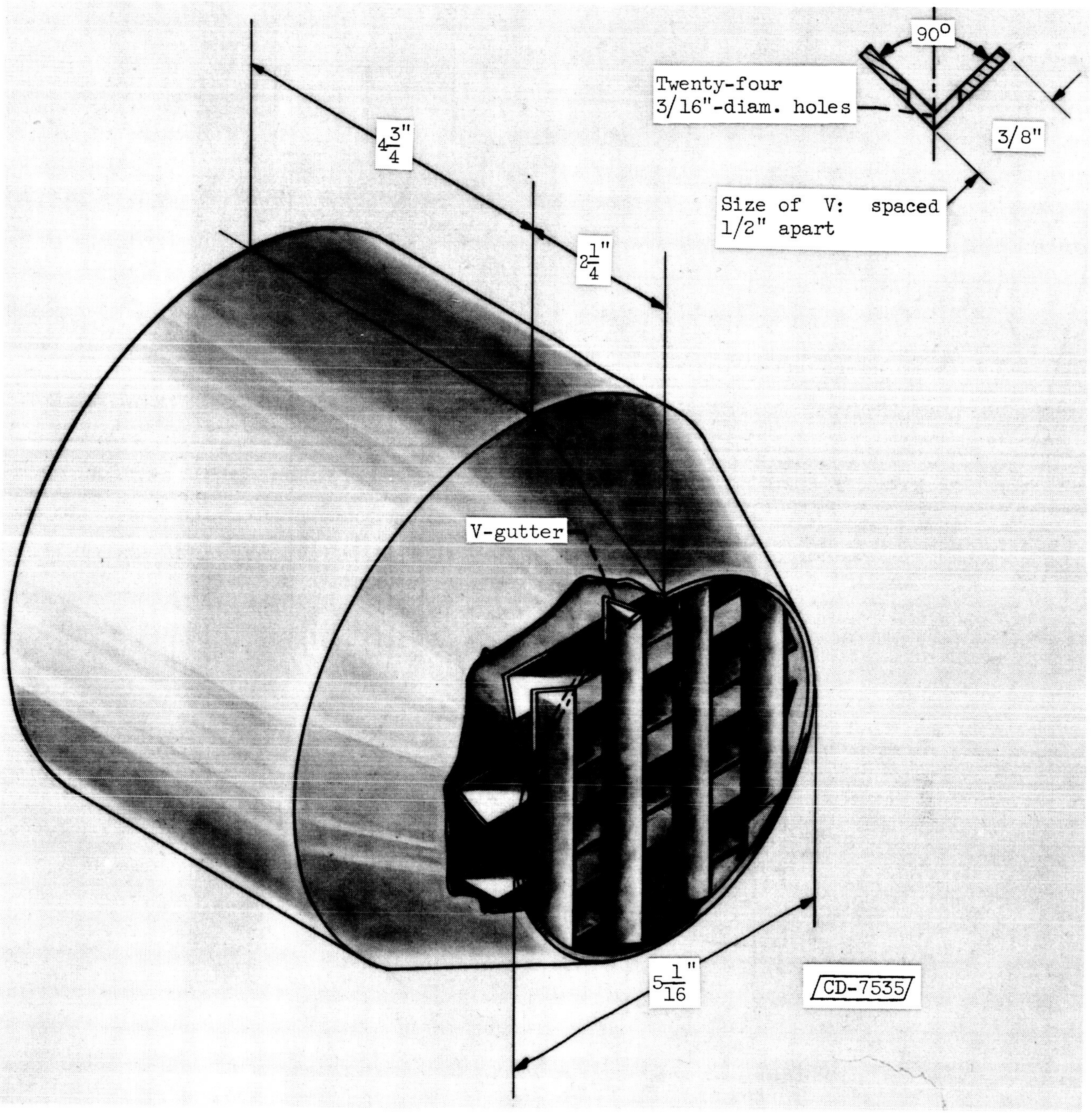
90°
Twenty-four
3/16"-diam. holes
3/8"
Size of V: spaced
1/2" apart
$4\frac{3}{4}$"
$2\frac{1}{4}$"
V-gutter
$5\frac{1}{16}$"
CD-7535

Figure 2. - V-gutter turbulence generator.

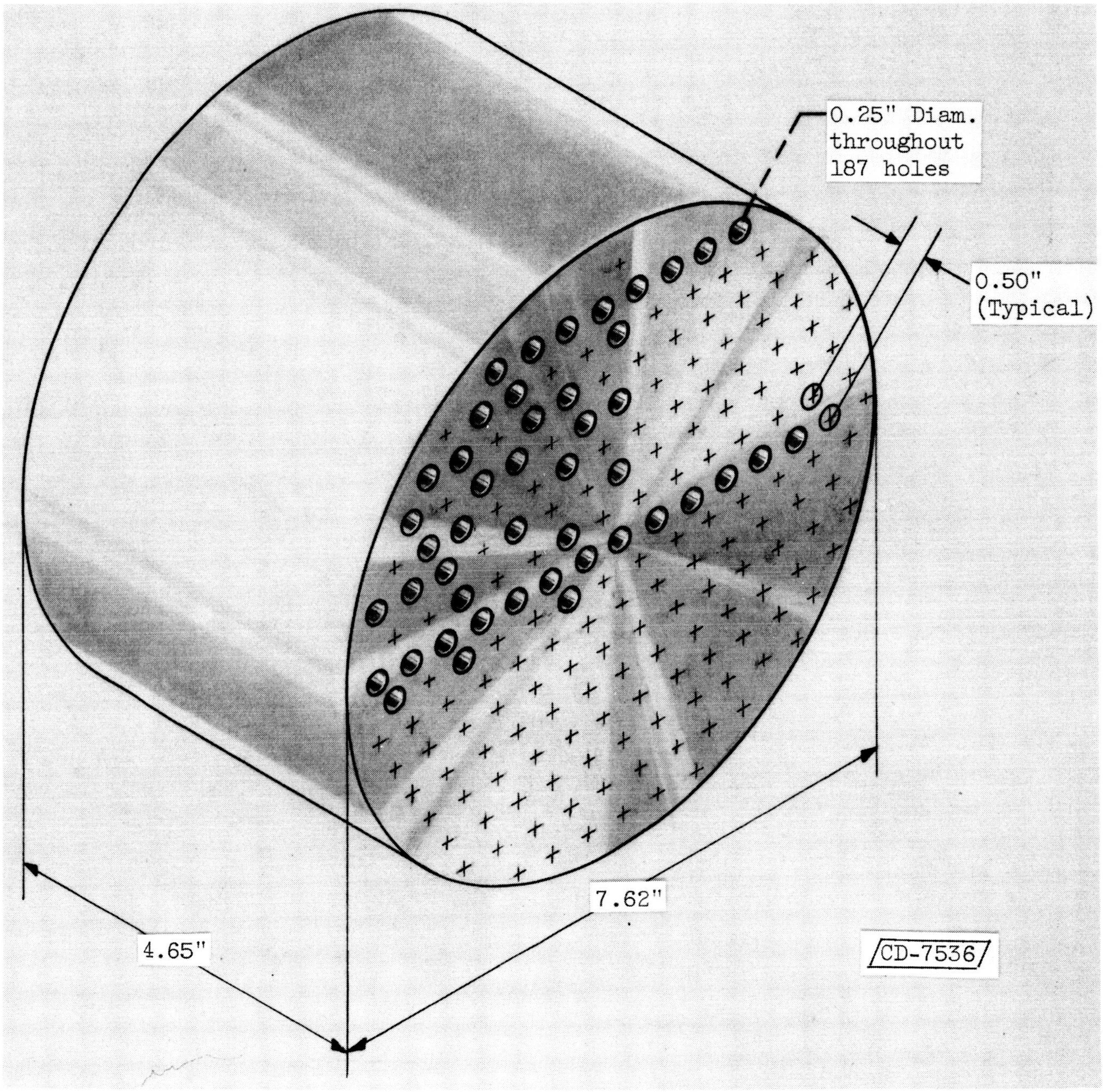
0.25" Diam.
throughout
187 holes
0.50"
(Typical)
7.62"
4.65"
CD-7536

Figure 3. - Nuclear-core simulator.

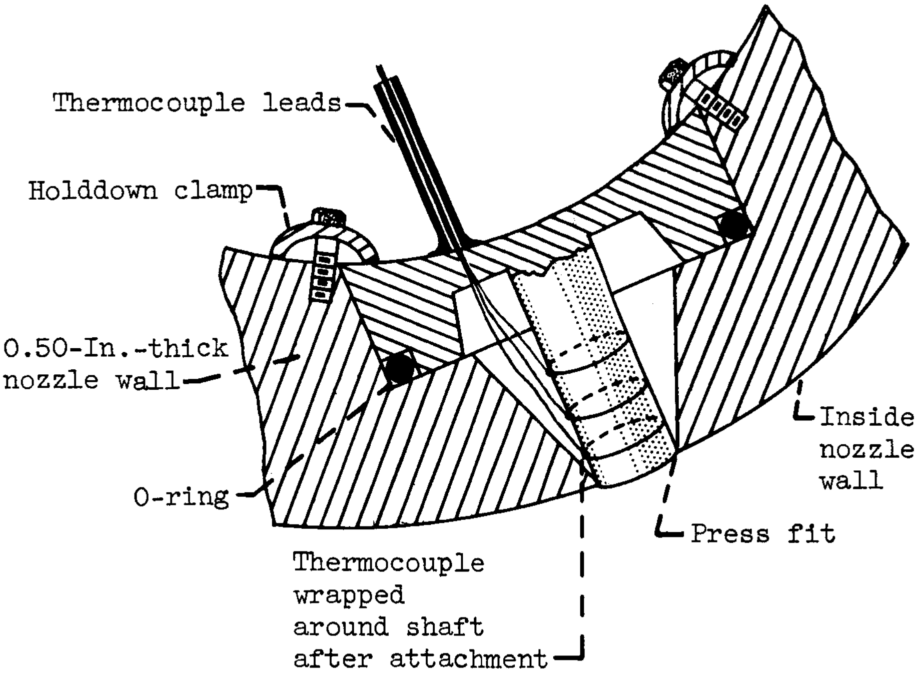
Thermocouple leads
Holddown clamp
0.50-In.-thick nozzle wall
O-ring
Thermocouple wrapped around shaft after attachment
Press fit
Inside nozzle wall

(a) Schematic diagram.

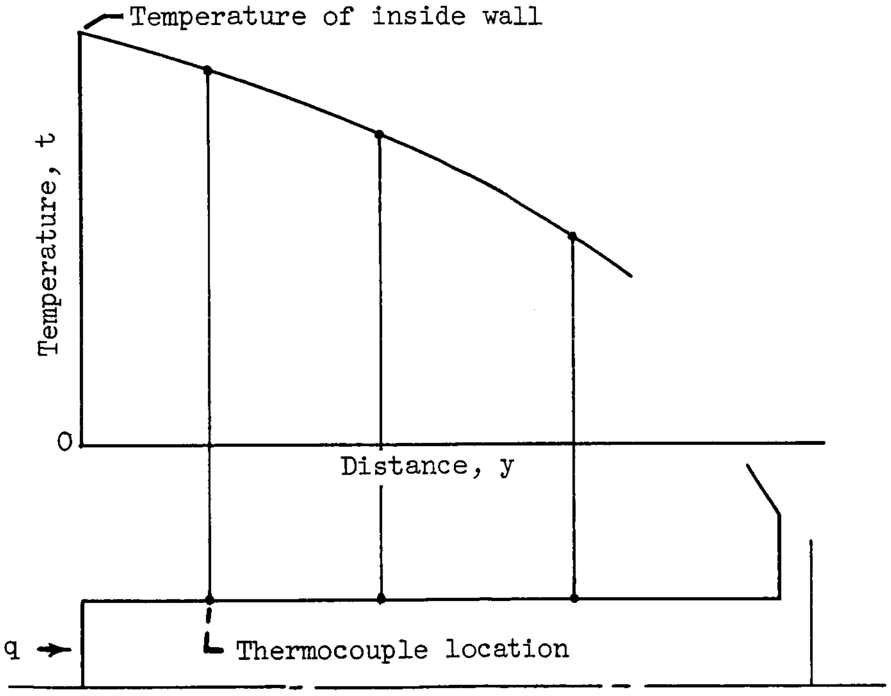
Temperature of inside wall
Temperature, t
0
Distance, y
q
Thermocouple location

CD-7621

(b) Typical measurements.

Figure 4. - Heat-flux meter.

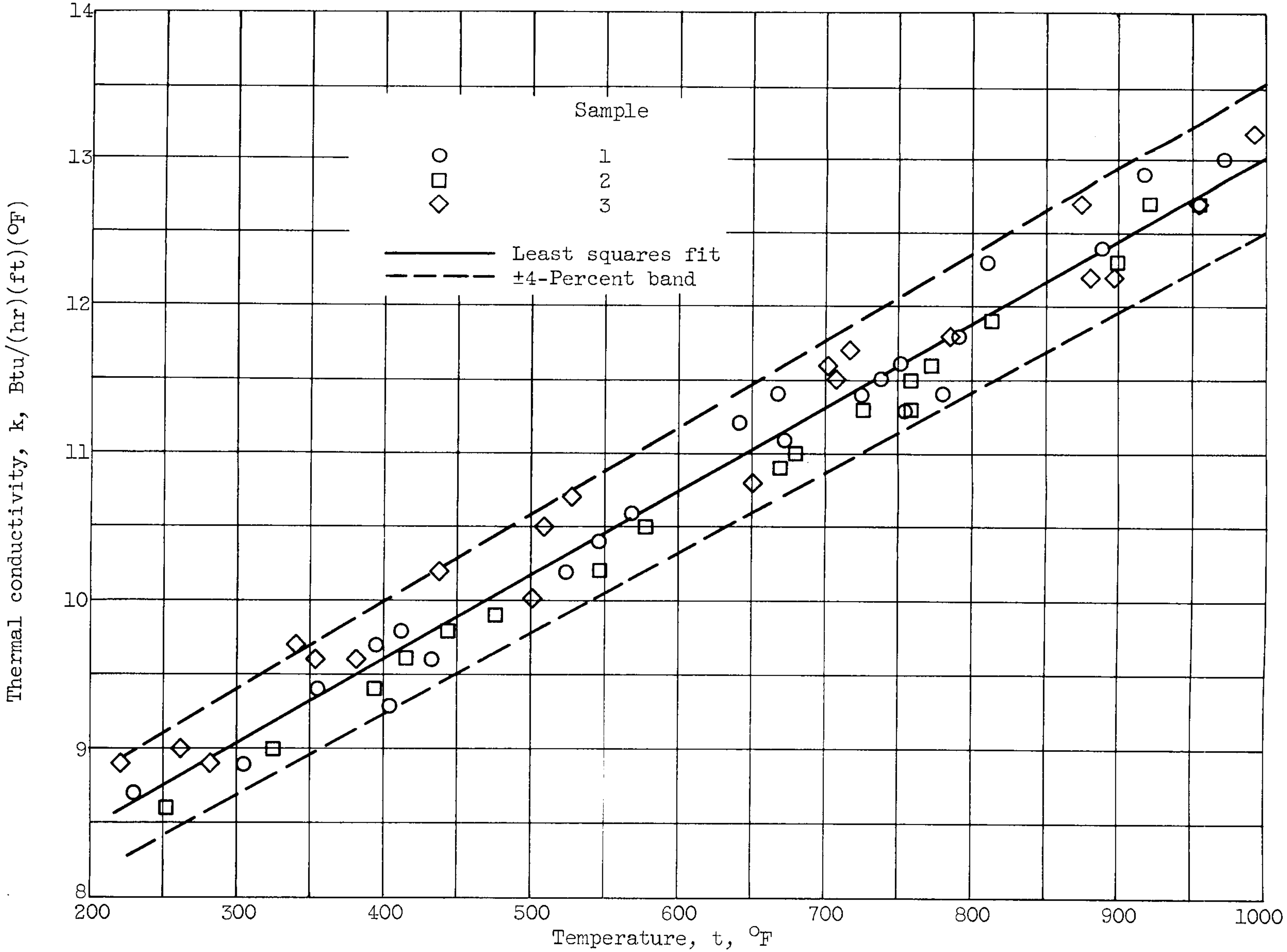

Figure 5. - Experimental thermal conductivity measurement of Inconel made by Battelle Memorial Institute. Samples 1 and 2 were annealed in a vacuum furnace at 1900° F for 15 minutes and then furnace cooled. Sample 3 had a temperature soak at 1950° F for 1 hour then was air cooled.

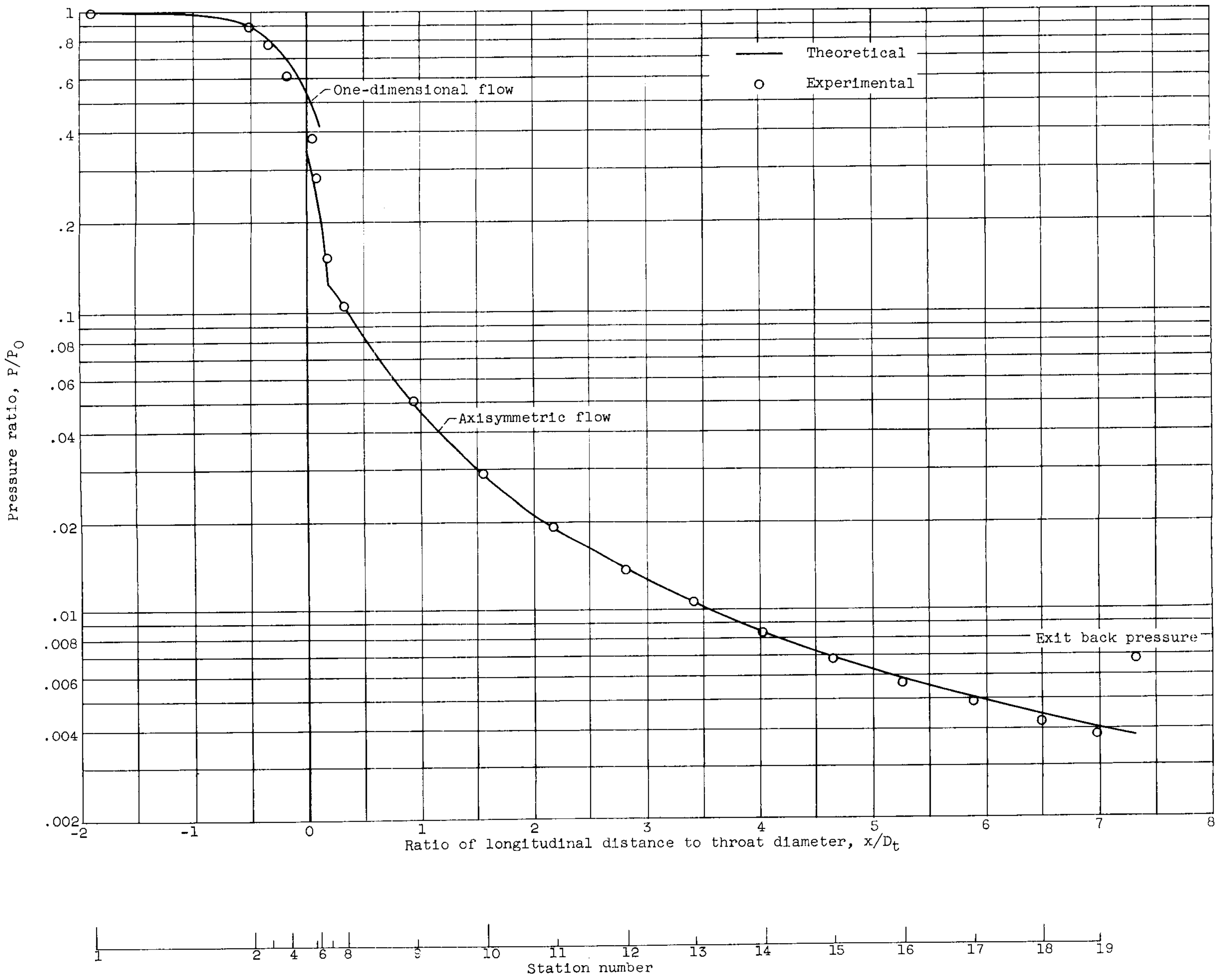

Figure 6. - Pressure ratio in a Rao nozzle with air. Total pressure, 300 pounds per square inch absolute; throat diameter, 1.624 inches.

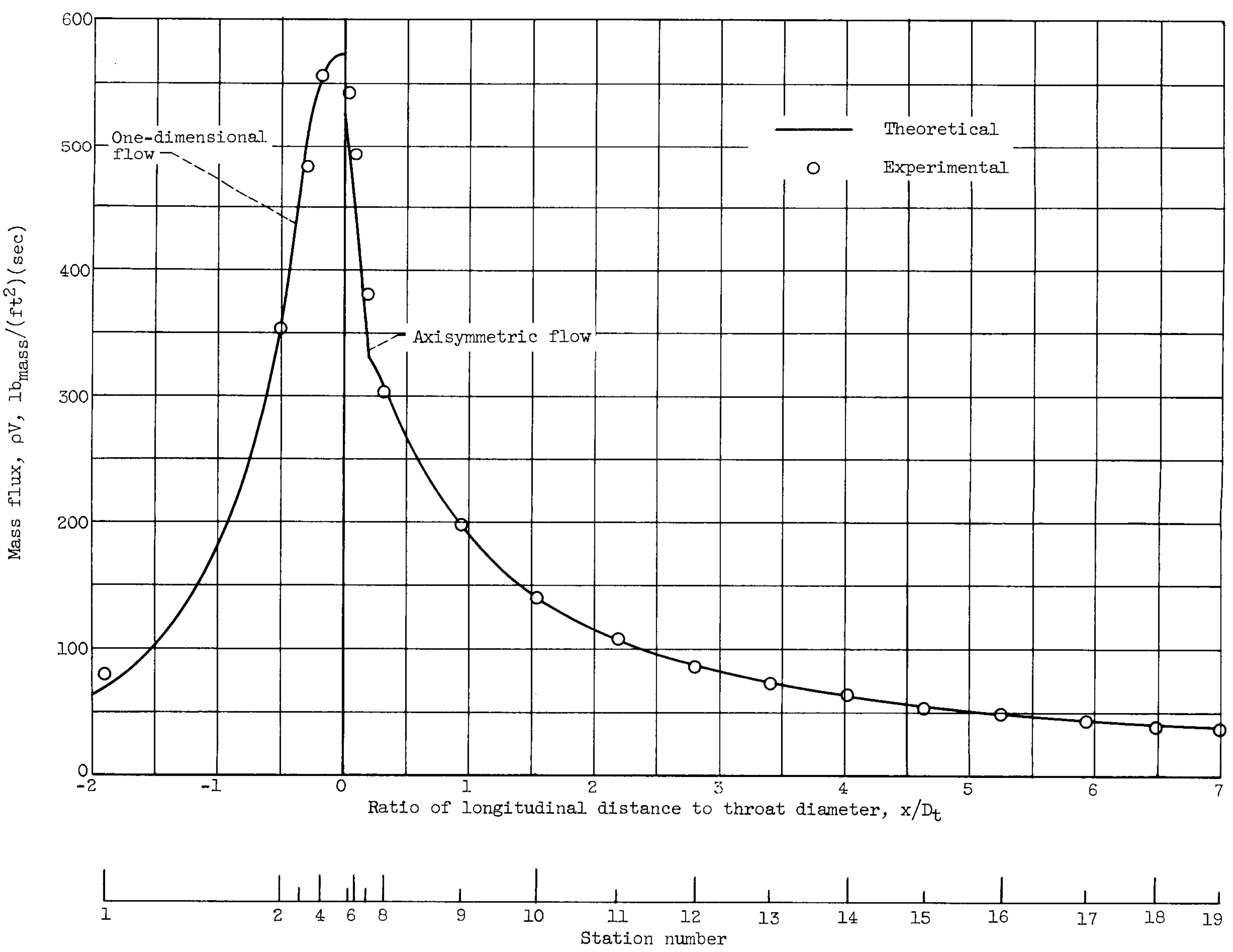

Figure 7. - Mass flux distribution at edge of boundary layer for truncated Rao nozzle with air. Total pressure, 300 pounds per square inch absolute; total temperature, 1620° R; throat diameter, 1.624 inches.

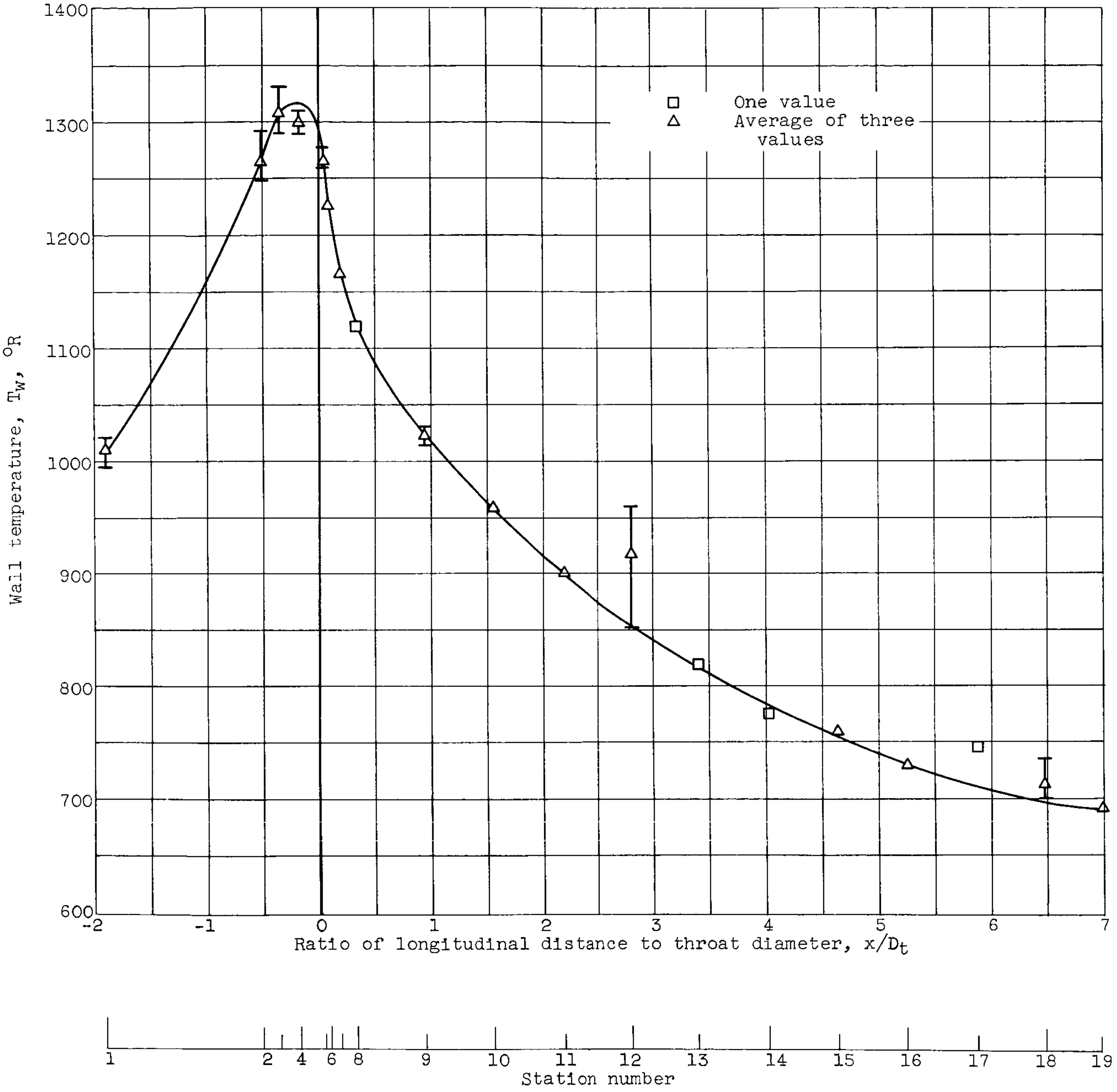

(a) Total temperature, 1607° R; total pressure, 300 pounds per square inch absolute. No upstream flow disturbance.

Figure 8. - Wall temperature distribution in a truncated Rao nozzle.

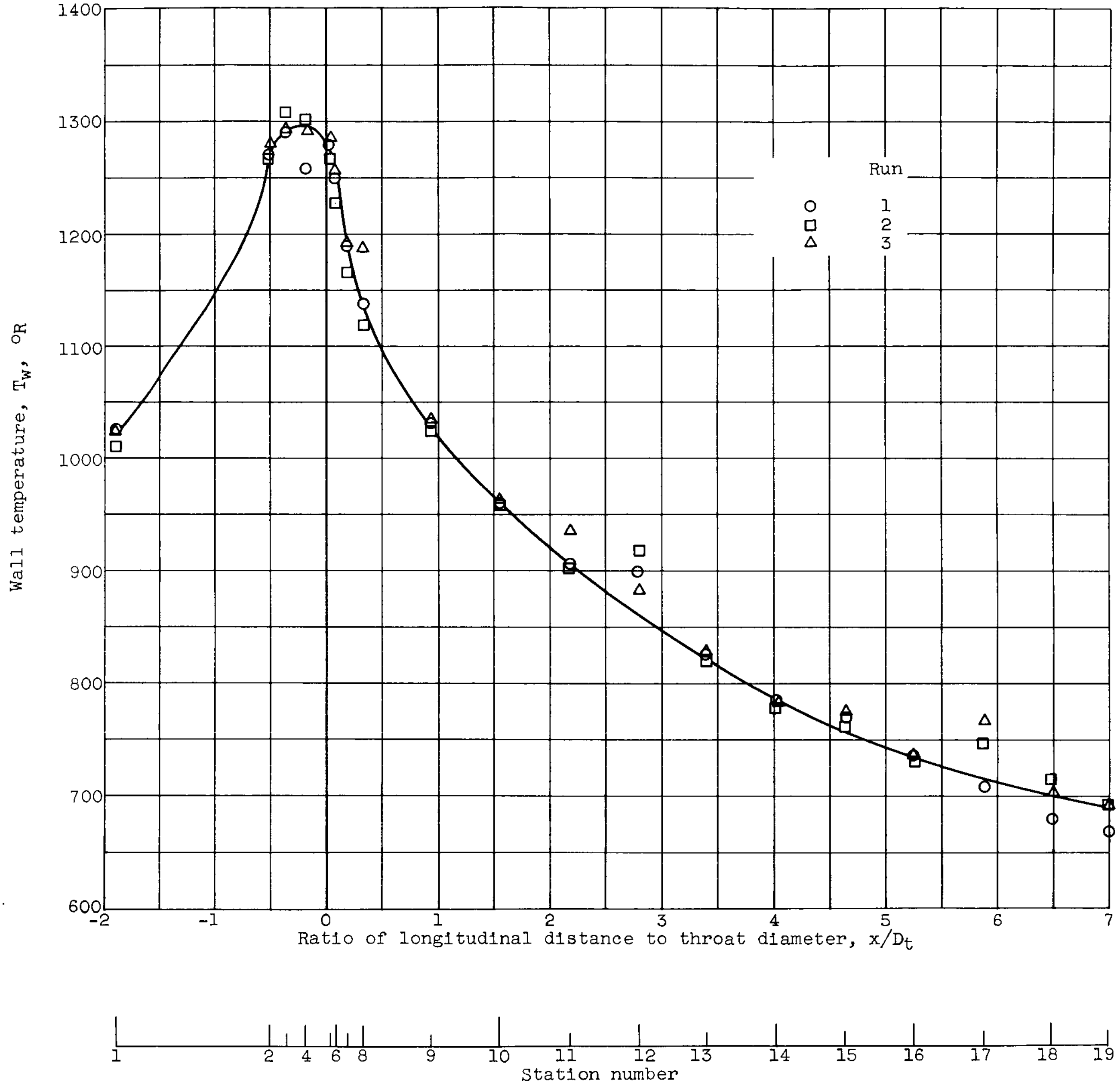

(b) Nominal total temperature, 1600° R; total pressure, 300 pounds per square inch absolute. No upstream flow disturbance.

Figure 8. - Continued. Wall temperature distribution in a truncated Rao nozzle.

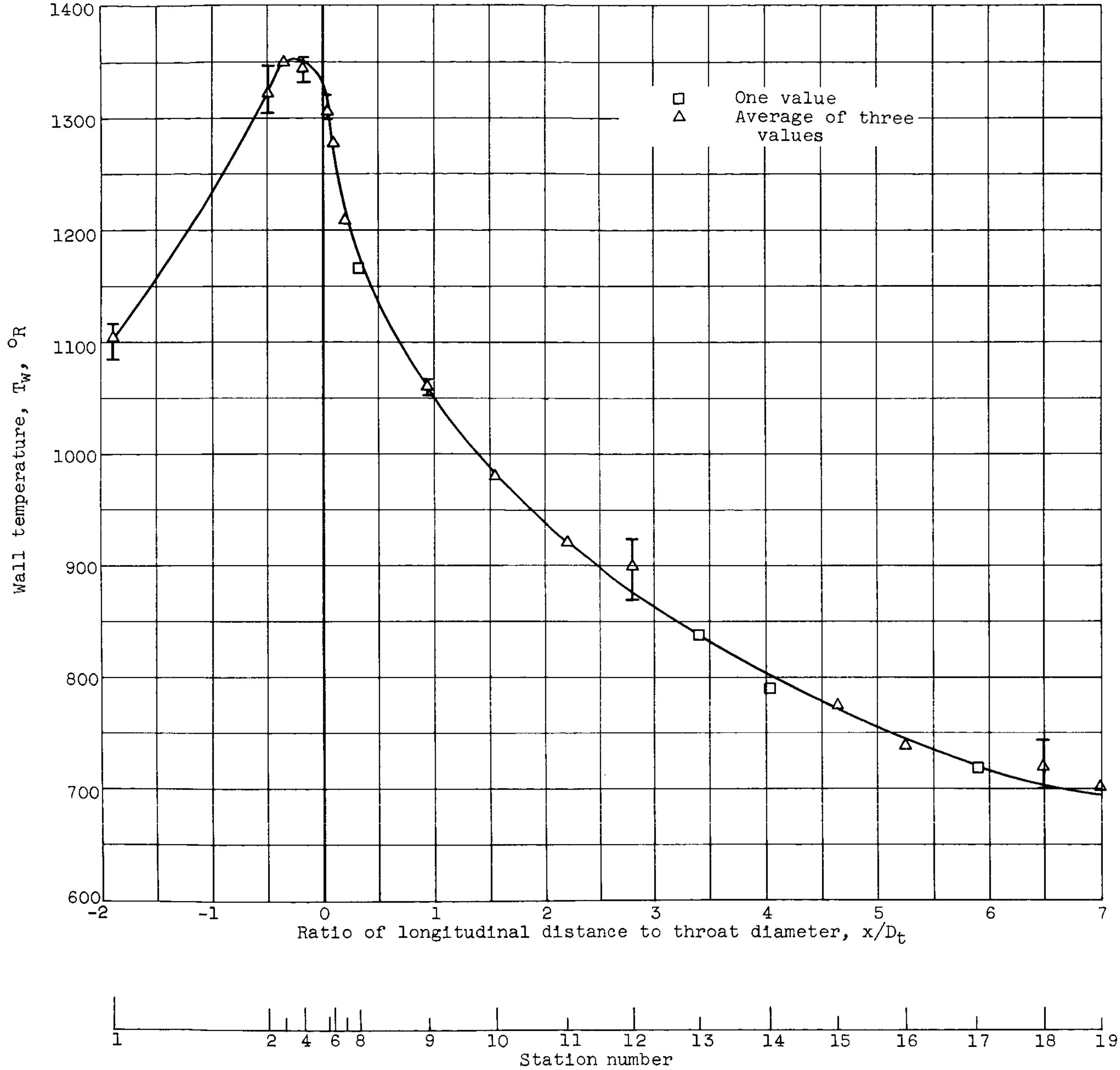

(c) Total temperature, 1605° R; total pressure, 302 pounds per square inch absolute. Upstream nuclear-core simulator.

Figure 8. - Continued. Wall temperature distribution in a truncated Rao nozzle.

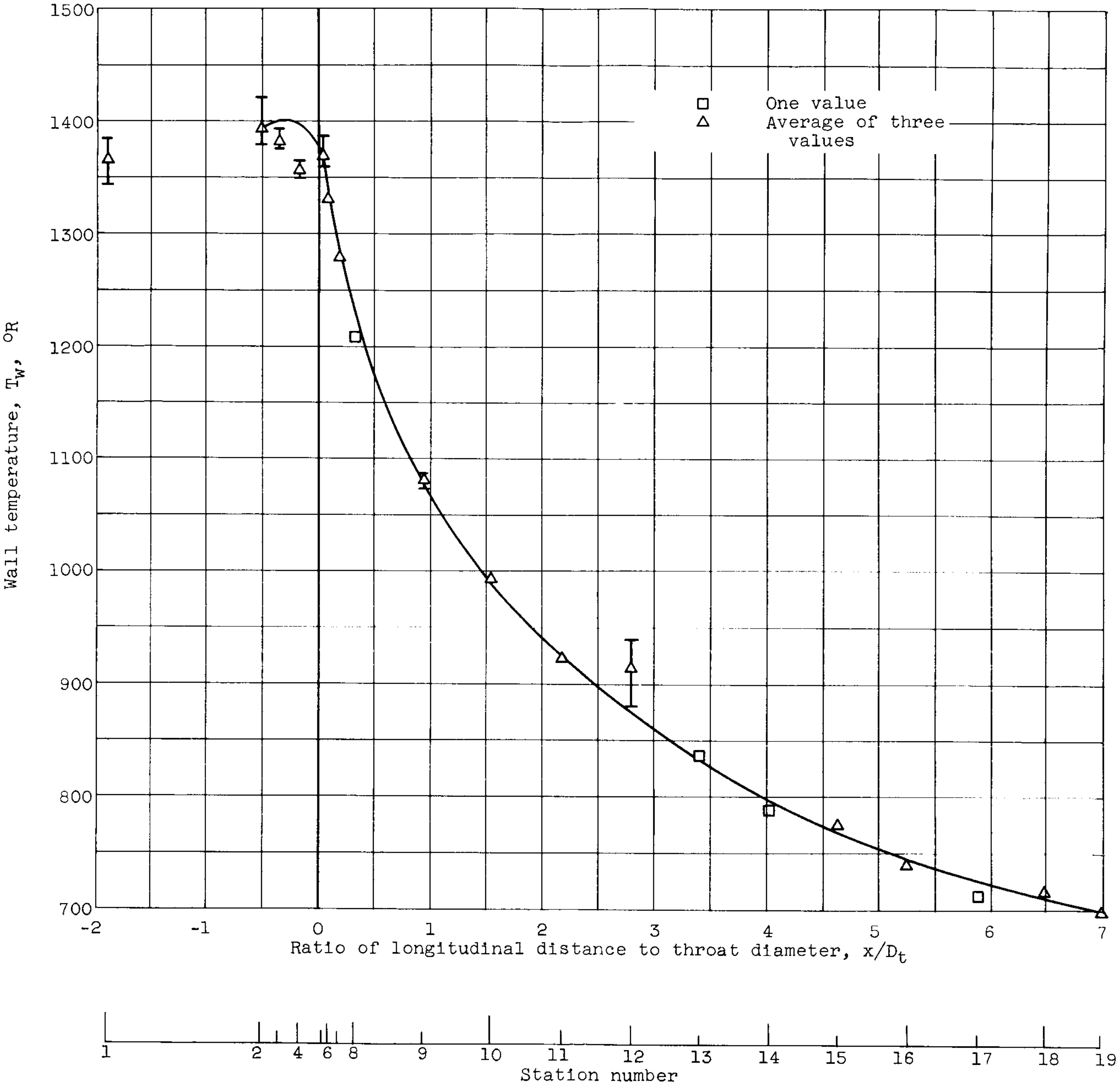

(d) Total temperature, 1612° R; total pressure, 302 pounds per square inch absolute. Upstream turbulence generator.

Figure 8. - Concluded. Wall temperature distribution in a truncated Rao nozzle.

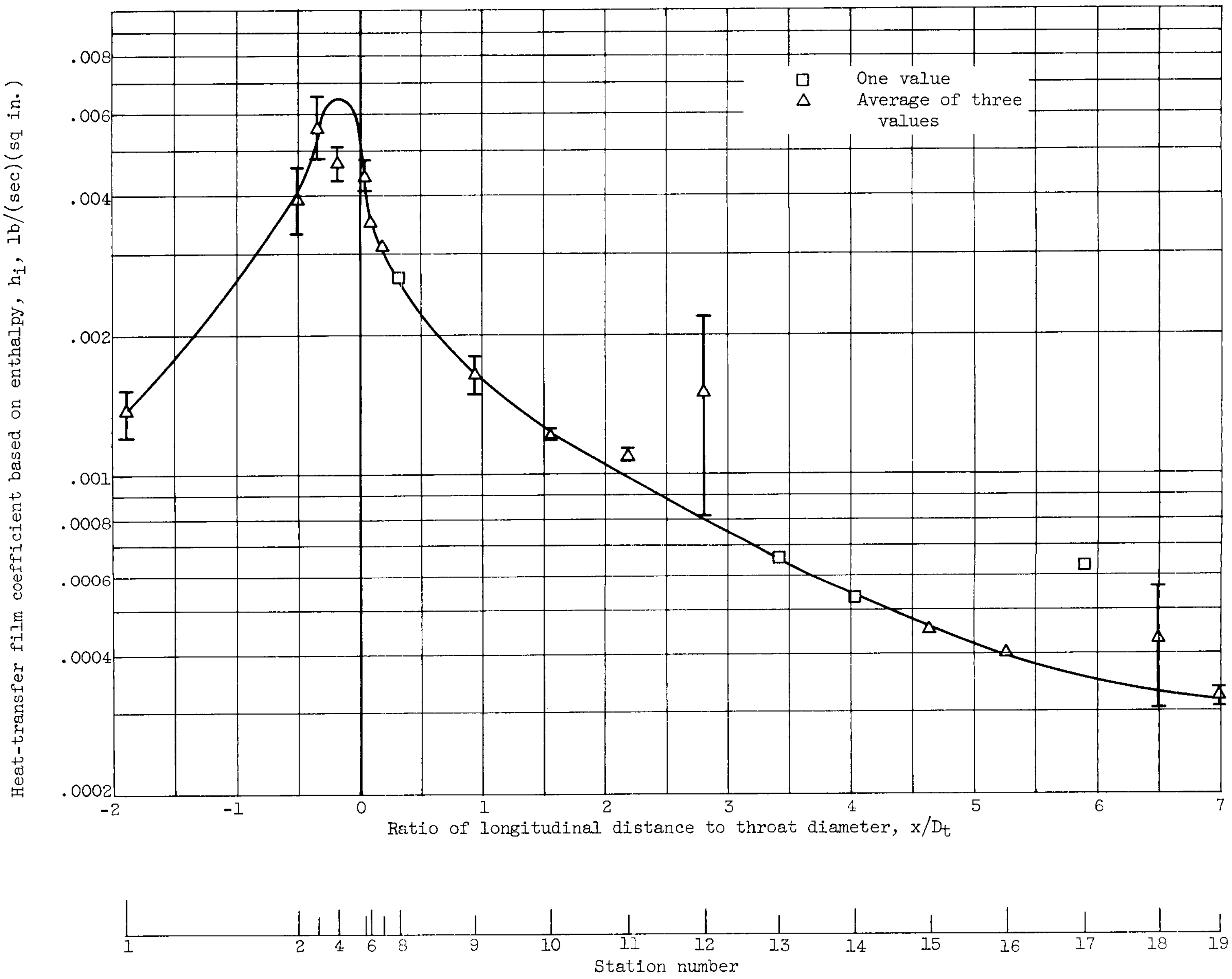

(a) Total temperature, 1607° R; total pressure, 300 pounds per square inch absolute. No upstream flow disturbance.

Figure 9. - Heat-transfer film coefficient in a truncated Rao nozzle.

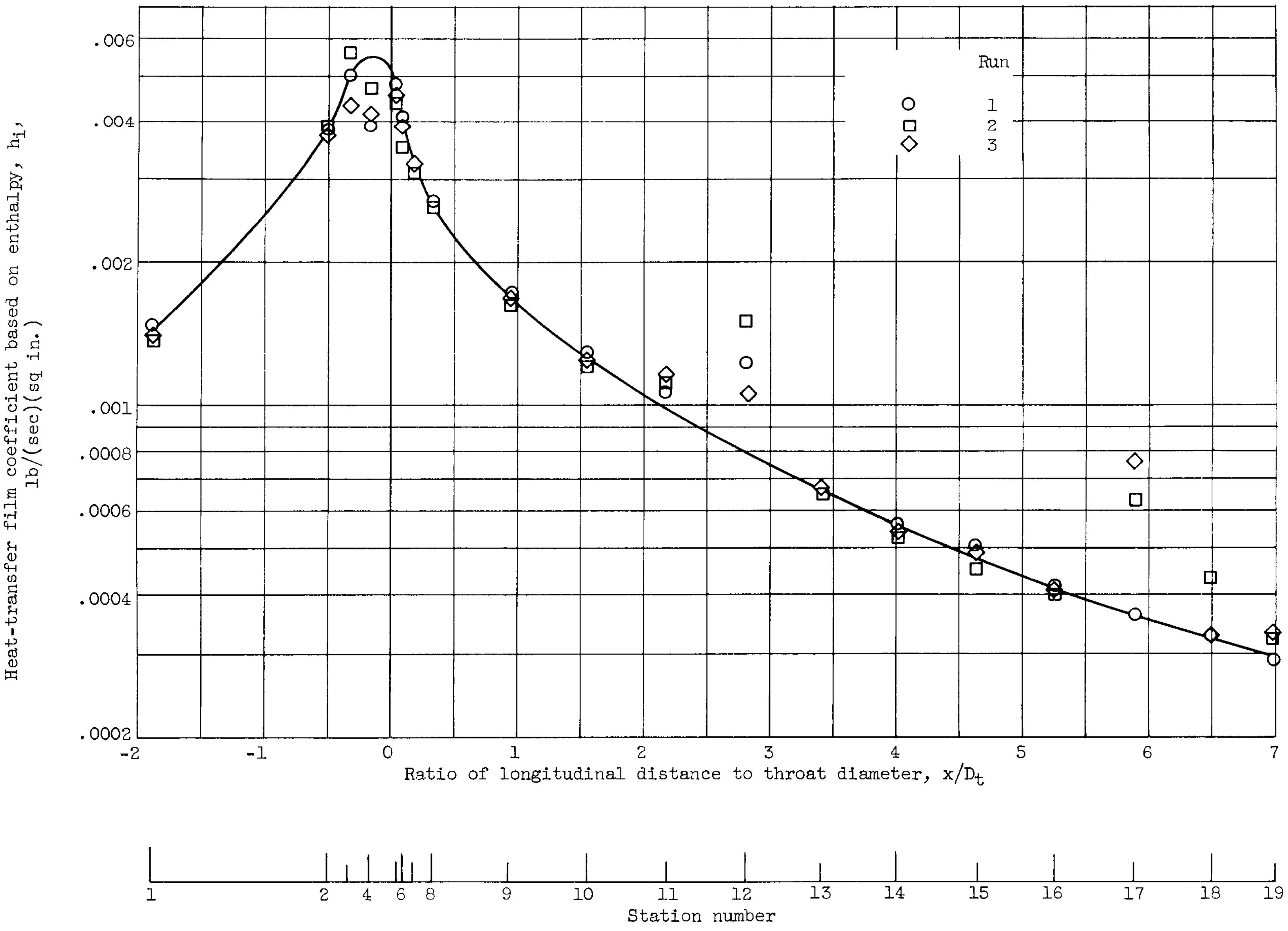

(b) Nominal total temperature, 1600° R; total pressure, 300 pounds per square inch absolute. No upstream flow disturbance.

Figure 9. - Continued. Heat-transfer film coefficient in a truncated Rao nozzle.

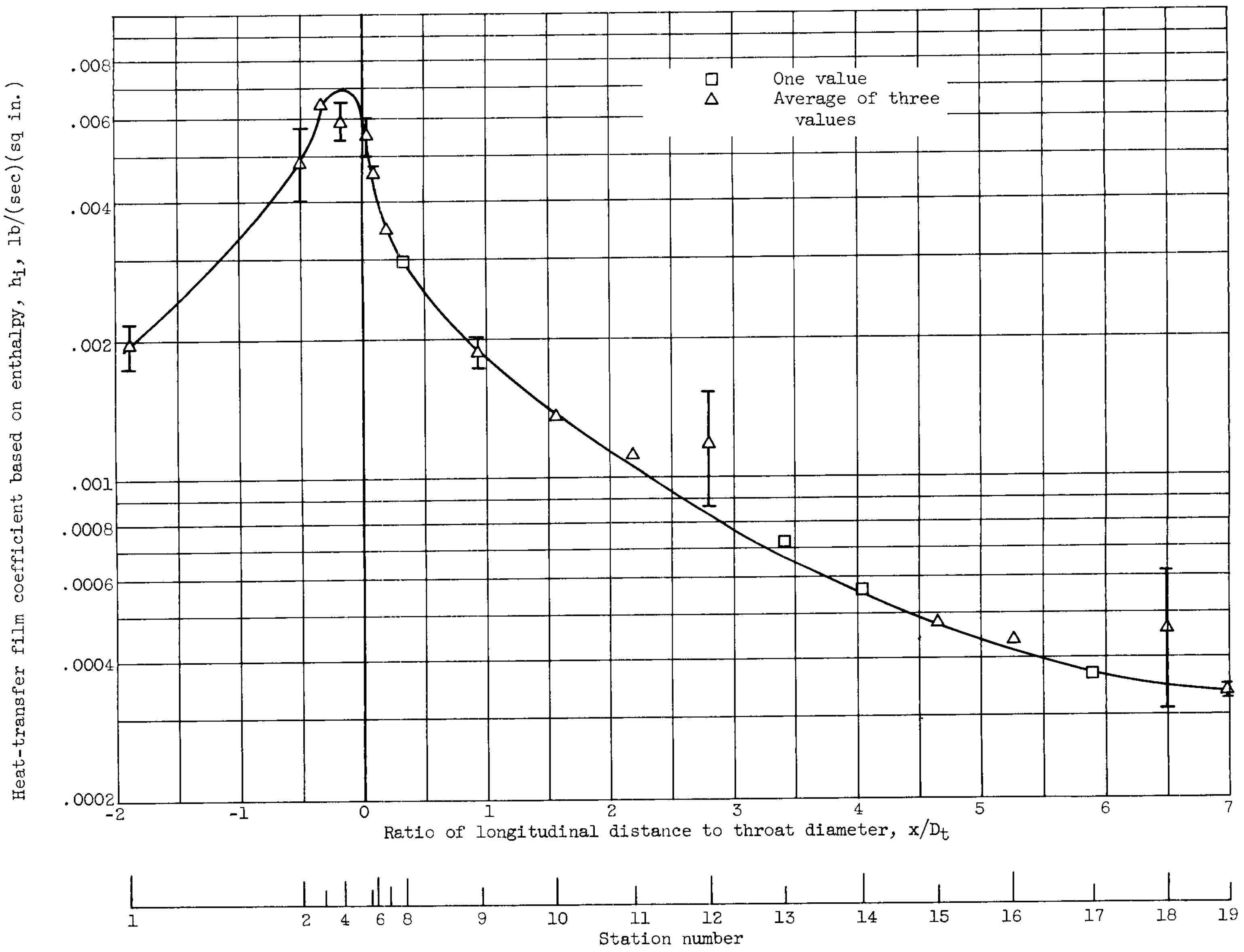

(c) Total temperature, 1605° R; total pressure, 302 pounds per square inch absolute. Upstream nuclear-core simulator.

Figure 9. - Continued. Heat-transfer film coefficient in a truncated Rao nozzle.

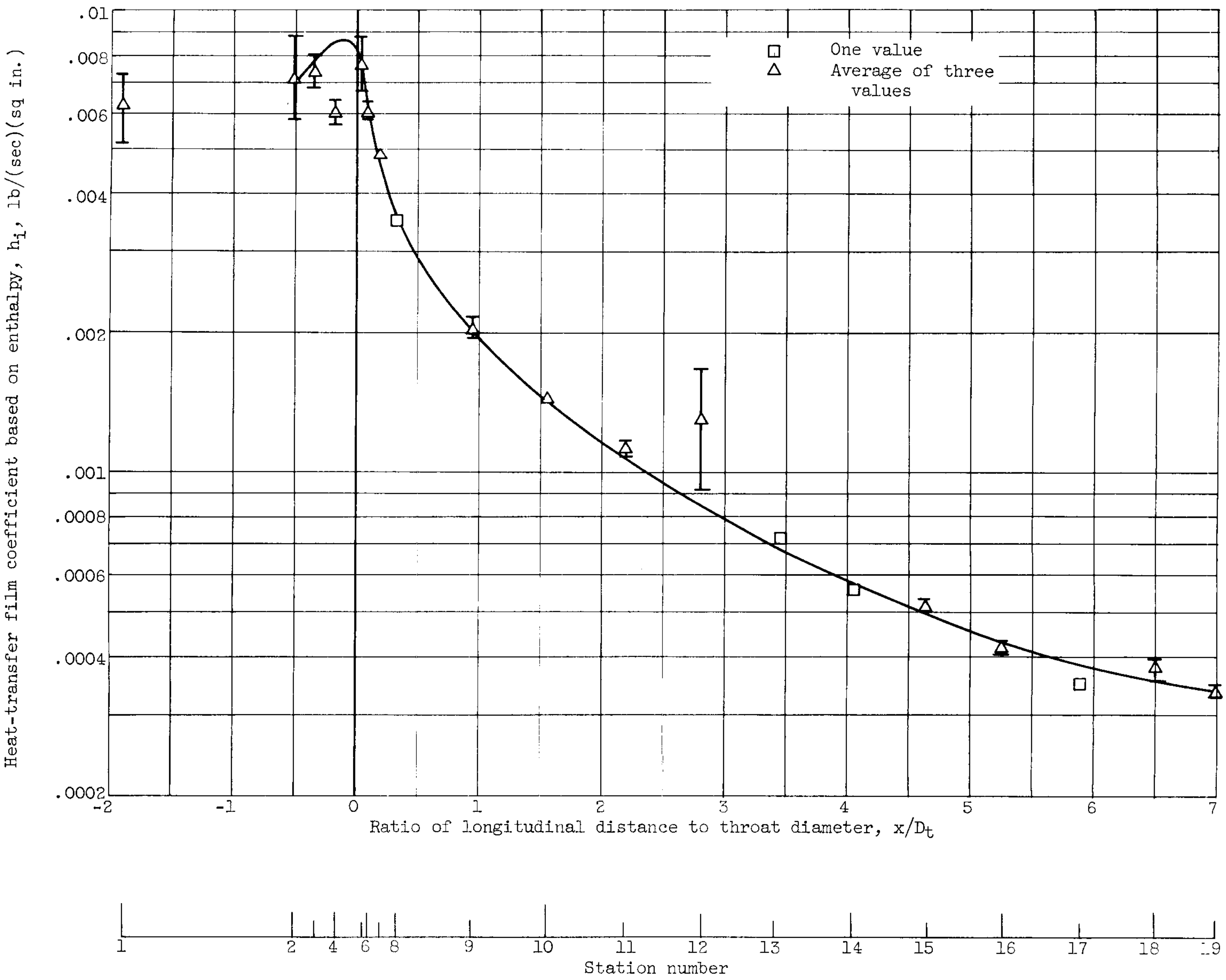

(d) Total temperature, 1612° R; total pressure, 300 pounds per square inch absolute. Upstream turbulence generator.

Figure 9. - Continued. Heat-transfer film coefficient in a truncated Rao nozzle.

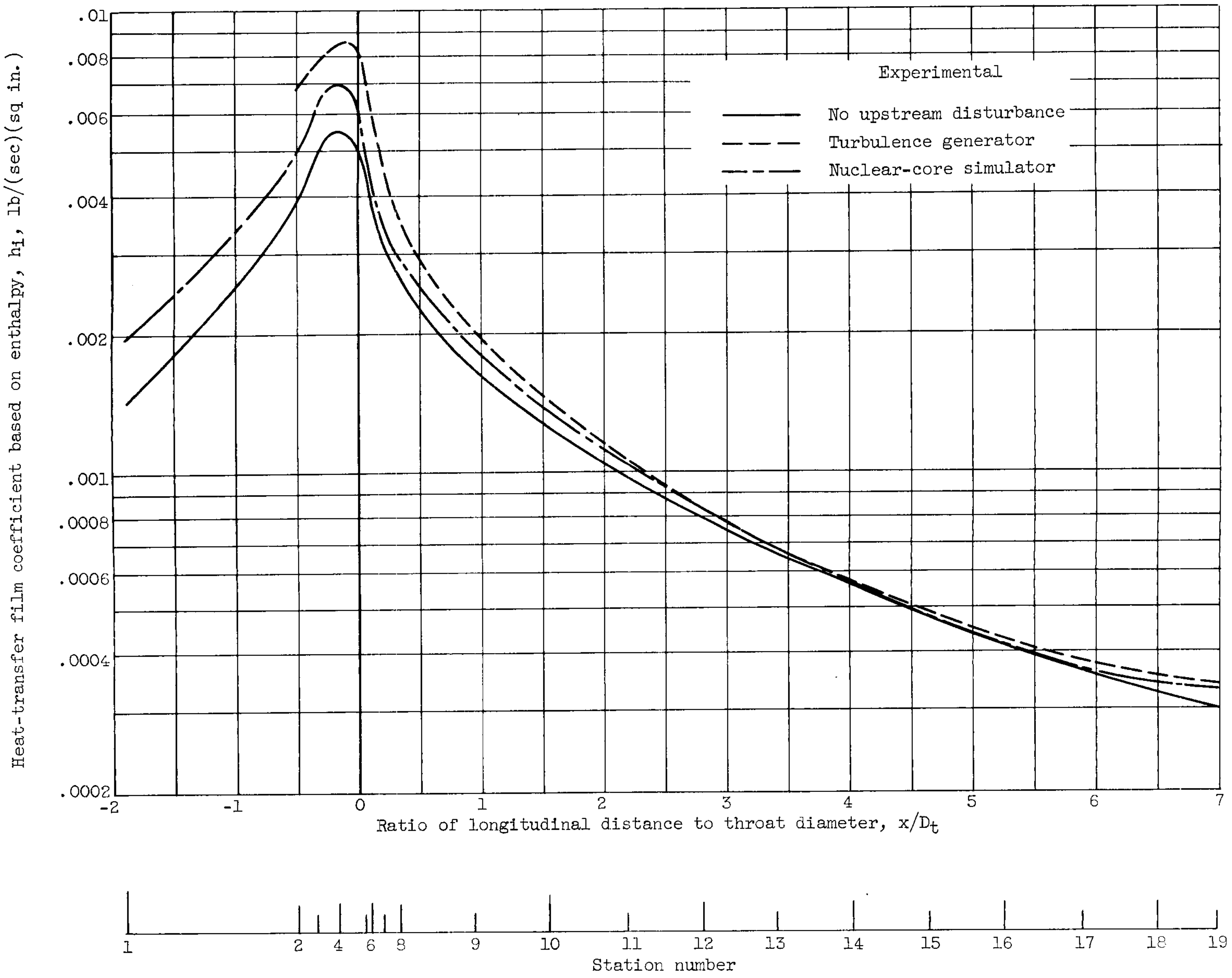

(e) Nominal total temperature, 1600° R; nominal total pressure, 300 pounds per square inch absolute.

Figure 9. - Continued. Heat-transfer film coefficient in a truncated Rao nozzle.

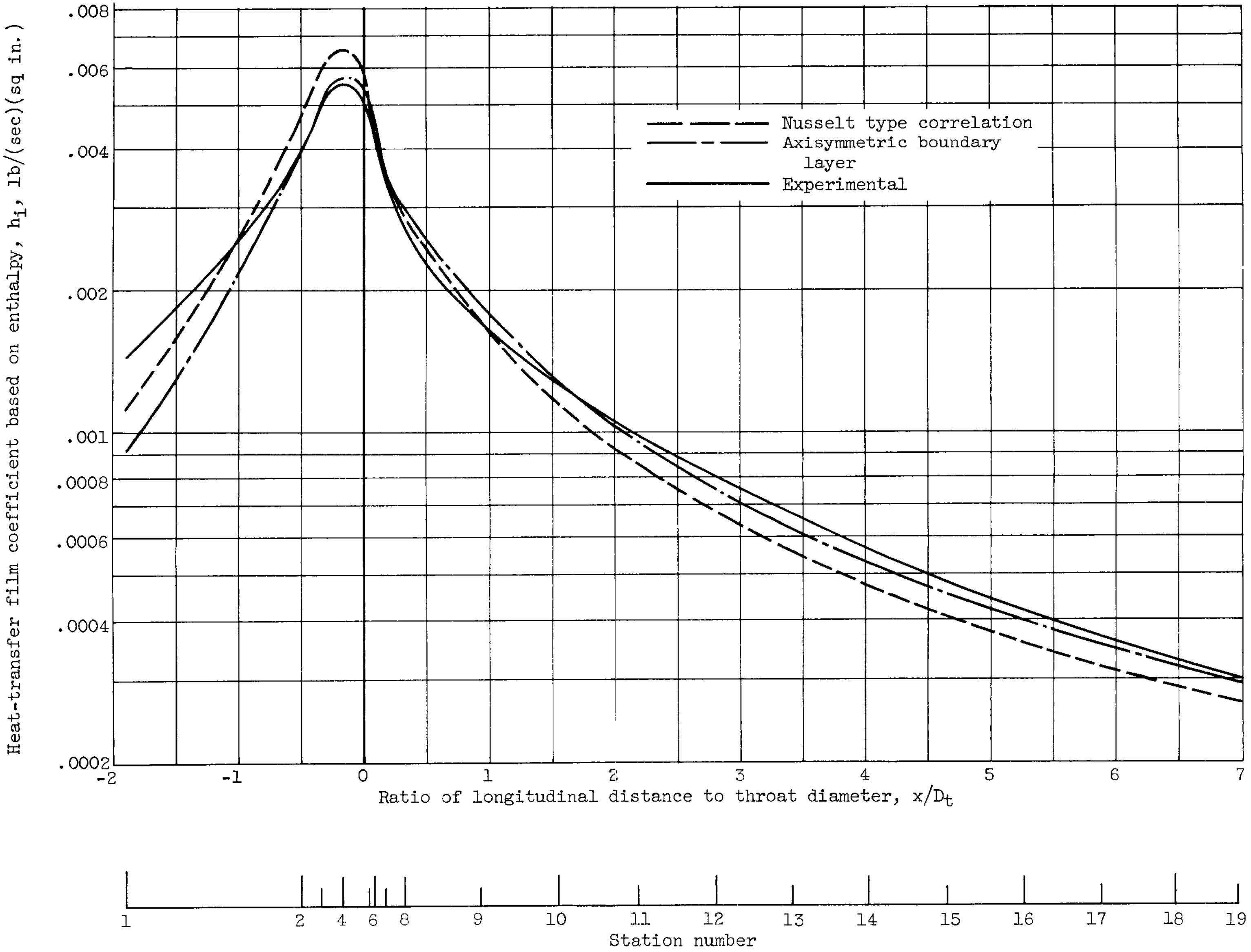

(f) Total temperature, 1600° R; total pressure, 300 pounds per square inch absolute. No upstream flow disturbance.

Figure 9. - Continued. Heat-transfer film coefficient in a truncated Rao nozzle.

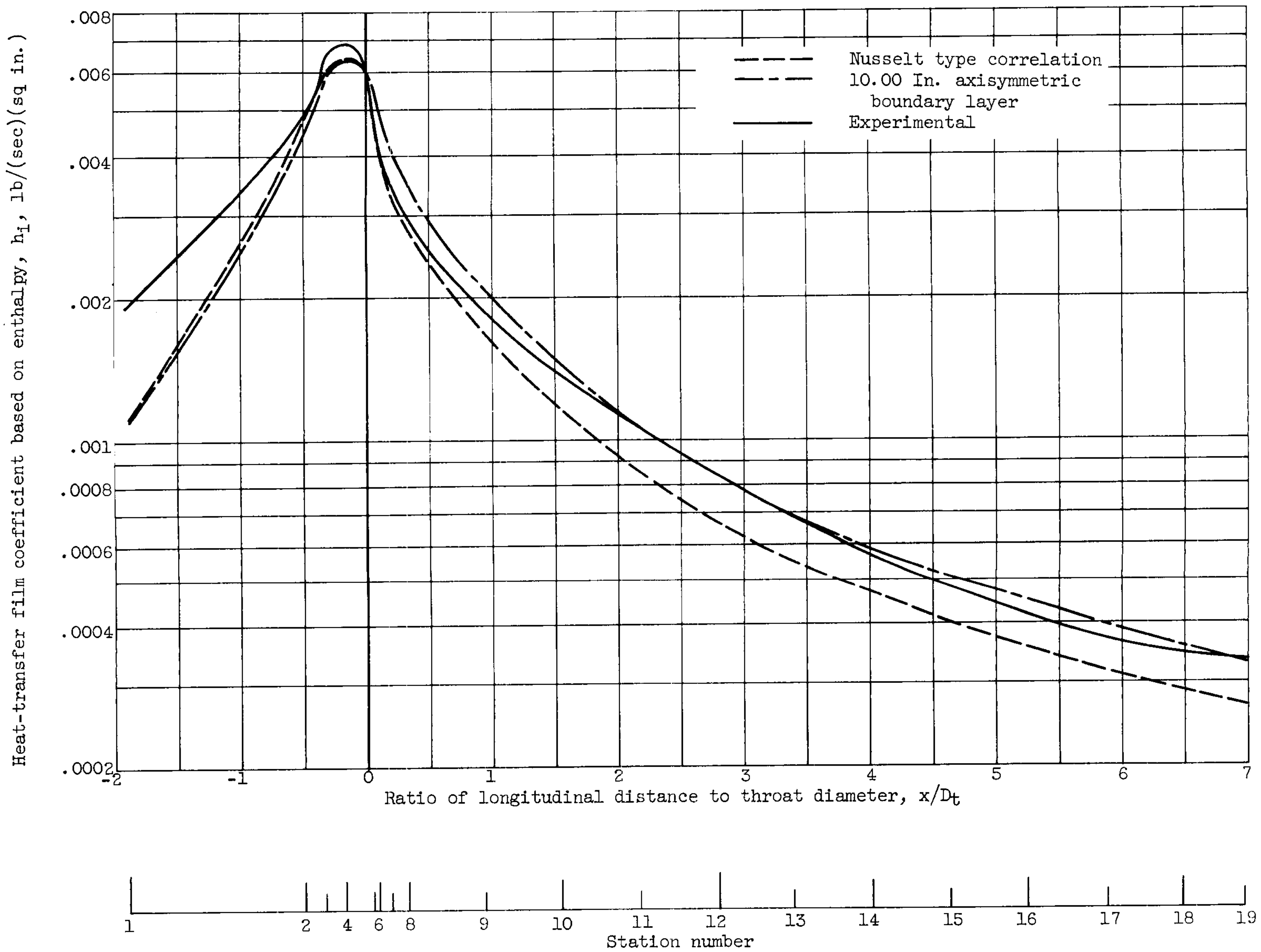

(g) Total temperature, 1605° R; total pressure, 302 pounds per square inch absolute. Upstream nuclear-core simulator.

Figure 9. - Continued. Heat-transfer film coefficient in a truncated Rao nozzle.

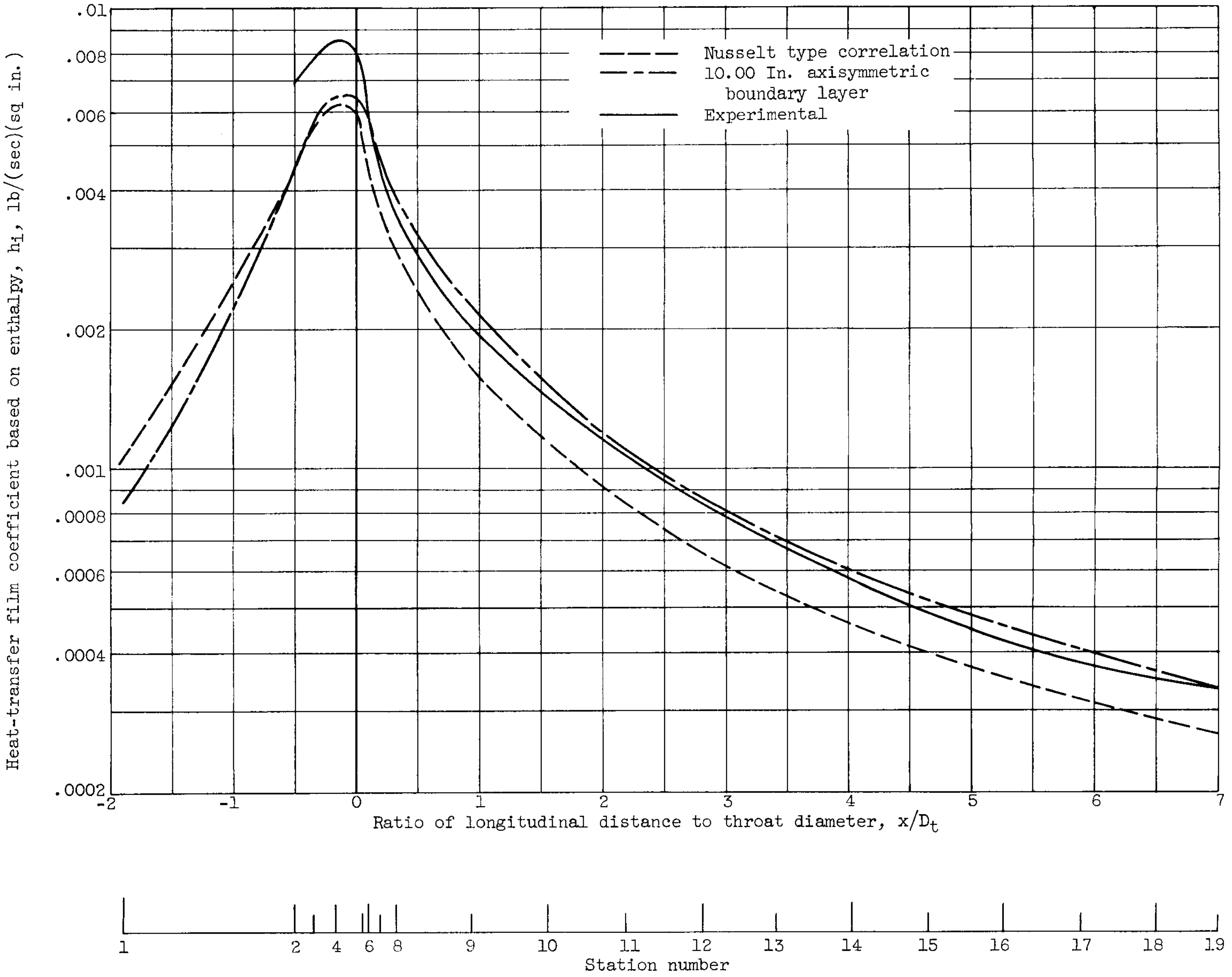

(h) Total temperature, 1612° R; total pressure, 300 pounds per square inch absolute. Upstream turbulence generator.

Figure 9. - Concluded. Heat-transfer film coefficient in a truncated Rao nozzle.

NASA-Langley, 1963 E-1851